RELATIVISTIC HEAVY-ION PHYSICS

DISSERTATION

SUBMITTED IN PARTIAL FULFILMENT OF THE REQUIREMENTS
FOR THE AWARD OF THE DEGREE OF

Master of Philosophy

IN

PHYSICS

BY

ARSHAD AHMAD

Under the Supervision of

Prof. Muhammad Irfan

DEPARTMENT OF PHYSICS
ALIGARH MUSLIM UNIVERSITY
ALIGARH (INDIA)

2007

To

My family

&

Friends

Dr. Muhammad Irfan.
Professor of Physics
Phone: +91-571-2700093
Fax: +91-571-2700093

Department of Physics
Aligarh Muslim University
Aligarh-202002
INDIA.

Email: hep_amu@rediffmail.com

CERTIFICATE

Certified that this dissertation entitled, " **Relativistic Heavy-Ion Physics** " embodies the original work of Mr. Arshad Ahmad carried out under my supervision. The work is worthy of consideration for the award of M.Phil. degree.

Mohd Irfan 9/10/07

(Prof. Muhammad Irfan)

Acknowledgments

Foremost, I would like to thank my respected supervisor, Prof.Muhammad Irfan for providing me an opportunity to work under his able guidance. His constant attention made me a better person academically as well as in other spheres of life.

I specially want to thank my senior colleagues Dr.Nazir Ahmad, Dr. M.Mohsin Khan, Mr. Danish Azmi and Mr. Arshad Kamal, whose support and guidance made this dissertation possible. I am very grateful for their patience, motivation and enthusiasm.

Special thanks are due to Prof M.Zafar for his constructive suggestions and moral support.

I acknowledge with gratitude various helps extended to me by my colleagues Mr. Urfi Farooqui and Kousar Saleem.

I also thank my friend Mr. Suhail Ahmad Siddiqui for his companionship during my stay at Aligarh.

Thanks are also due to Mr.S.M.Mahir and Er.Khalid Imdad for extending their technical help.

I have no words to acknowledge the kind of support and encouragement provided to me by my friends and my family. They have been there for me always, whenever I needed them.

ARSHAD AHMAD

CONTENTS

List of Figures

List of Tables

CHAPTER I

Introduction

1.1 Background :

The primary motivation for studying nucleus-nucleus collisions at relativistic and ultra-relativistic energies is to investigate matter at higher and higher energy densities ($\epsilon >> 1GeV/fm^3$). The system created in these high-energy heavy-ion collisions reach energy densities close to the "critical" value of about 1.5-3 GeV/fm^3, corresponding to temperatures lying in the range 150-190 MeV, where lattice QCD predicts a phase transition to take place to a deconfined state of quarks and gluons- the Quark-Gluon Plasma (QGP) as indicated [1] in the phase diagram Fig.1.1. The study of the phase diagram of strongly interacting matter will help address some basic questions relating to the origin of hadron masses, restoration of chiral symmetry, structure of neutron stars, supernova dynamics and the early Universe.

QGP is believed to have existed in the early Universe [2], just before few microseconds after the Big Bang and is also believed to exist in the core of the neutron stars[3]. However, the only possibility to study quark-gluon plasma in the laboratory is through the collision of heavy nuclei at relativistic energies [4-7].

By the mid-1980s, as the design of the RHIC (Relativistic Heavy Ion Collider) was being finalised, the first ultra-relativistic nuclear beams became available. Silicon and Gold ions were accelerated to 10 GeV/nucleon at Brookhavens Alternating Gradient (proton) Synchrotron (AGS). In Switzer-

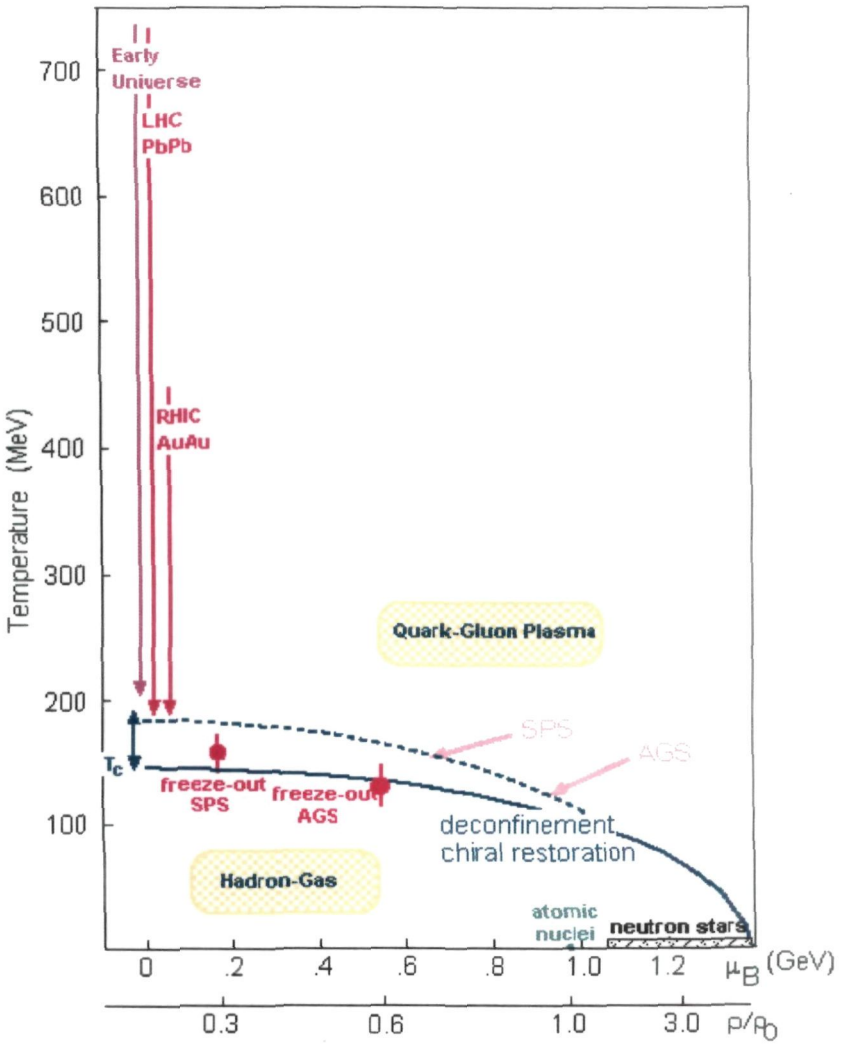

Fig 1.1 QCD Phase Diagram.

land, the CERN Super Proton Synchrotron (SPS) began providing 160-GeV/nucleon beams of Sulphur and Lead nuclei. But as these were fixed target experiments, they provided modest centre-of-mass energies of 5 and 17 GeV per nucleon pair respectively. Although the AGS and SPS centre-of-mass energies were far below than that of RHIC (Where the centre-of-mass energy between nucleons in Au-Au collision is 200 GeV), they provided the first opportunity for extensive studies of heavy-nucleus interactions at collision energies high enough to produce particles in abundance. The AGS and SPS fixed target experiments measured the abundances and spectra of many species of particles produced in heavy-ion collisions. The results obtained from these experiments

clearly indicated that relativistic nucleus-nucleus collisions are very different from a simple superposition of nucleon-nucleon interactions. These experiments have substantiated the expectation that heavy-ion experiments are an appropriate tool to create equilibrium hadronic matter and eventually the quark gluon plasma.

After fixed target experimental programs at BNL-AGS and CERN-SPS, RHIC has become the new high-energy frontier in the study of heavy-ion collisions. In June 2000, RHIC reported the first collisions between Gold nuclei at centre-of-mass energies of $\sqrt{S_{NN}} = 65$ GeV per nucleon-nucleon pair. In 2001, the first collisions at the maximum RHIC energy of $\sqrt{S_{NN}} = 200$ GeV were recorded which is about 10 times higher than that produced at AGS or SPS. The first data from RHIC have revealed certain exciting and qualitatively novel features like increased initial energy densities and temperatures, jet quenching, j/psi production, possibility of pentaquarks etc., and represent a major advance of heavy-ion physics in the ultra-relativistic energy regime.

The LHC is expected to be operational in 2008 with Pb ions at a centre-of-mass energy of about 6.4TeV per nucleon pair. While LHC is primarily a proton-proton collider, it will feature a heavy-ion program from day one with the dedicated ion experiment, ALICE. Extrapolating present results, it is evident that at LHC all the parameters relevant to the formation of QGP like the enegy density, size and lifetime of the system, etc., will be more favourable. At LHC, particle densities of several thousand per unit rapidity , a freeze out volume approaching 100,000 fm^3 and an initial temperature close to 1000 MeV is expected [8]. Another unique feature of heavy-ion physics at LHC is the pos-

sibility of measuring a large number of observables with very high precision on an event-by-event basis : impact parameter, multiplicity, particle ratios, spectra and various other important observables.

Nothing can be said unambiguosly about the formation of QGP and other exotic phenomena at the collision energy considered in the present study. However, an extensive and critical analysis on the data can pave a way to a clear understanding of the collision dynamics. Study of collisions at relativistic energies involving nuclear targets enable us to investigte the space-time development of the formation of secondary particles. Some definite and interesting conclusions regarding the mechanism of particle production can be drawn by studying various aspects of multiplicity of relativistic charged particles produced in nuclear collisions at different incident energies, for example, mean multiplicity, multiplicity distribution and its dispersion, thier dependence on the projectile energy and masses of the target and projectile nuclei, etc. Thus systematic and thorough investigation of emission characteristics of secondary particles producing black, grey and shower tracks will lead to a better understanding of the processes involved in nucleus-nucleus collisions at relativistic energies.

In the present study mechanism of multiparticle production is investigated by analyzing various emission characteristics of 14.5 A GeV/c ^{28}Si-beam emulsion interactions. Details about the stack used, scanning procedure and various measurements carried out in the present study are discussed in Chapter II.

Various characteristics of nucleus-nucleus collisions at 14.5 A GeV/c like multiplicity of producd particles, multiplicity distributions and correlations

among the produced particles are presented in Chapter III. The dependence of these observables on the projectile energy and the target mass have also been discussed.

Results on rapidity gap distributions have been presented in chapter IV. This aspect has been investigated to see any possible formation of intermediate clusters in the nucleus-nucleus collisions. This is based on the simple idea that particles coming from a cluster will lie close in the rapidity space. Attempt is also made to determine the cluster size and the number of clusters present in an interaction. Furthermore, the dependence of these aspects on the target mass and multiplicity of relativistic charged oparticles, n_s, has also been looked into.

The concluding chapter summarizes various results obtained in the present study.

1.2 Models of Nucleus-nucleus collisions :

The study of multiparticle production at high energies has been one of the most extensively studied topics in the recent years. From time to time, various models have been put forward to explain the mechanism of particle prouction in high energy heavy-ion collisions. Some of the models have been briefly described below.

1.2.1 Wounded Nucleon Model :

The success of the Wounded Nucleon Model in the description of general characteristics of hadron-nucleus collisions over a wide energy range has been remarkable. The average charged particle multiplicity in hadron-nucleus collision exhibited a slow increase than the number of individual nucleon-nucleon

collisions in various experiments at Fermilab [9], NA5 experiment and different emulsion data. This number, denoted usually by 'v' is given by:

$$v = A\frac{\sigma_{hp}}{\sigma_{hA}} \tag{1}$$

and the data gives the following dependence of the ratio of charged particles produced in hadron-nucleus and hadron-proton collisions as :

$$R = \frac{\langle n \rangle_{hA}}{\langle n \rangle_{hp}} = \frac{(1+v)}{2} \tag{2}$$

This is just the ratio of the number of participants in hadron-nucleus and hadron-proton collisions[9]. In its original form, Wounded Nucleon Model envisages that the particle production in nucleus-nucleus collision can be represented as a superposition of independent contribution from the wounded nucleons in the projectile and in target. Consequently, density of particles in a collision of nuclei of mass numbers A and B is given by [10]:

$$\frac{dN_{AB}}{dy} = w_A F_A(y) + w_B F_B(y) \tag{3}$$

where w_A and w_B are the nos. of wounded nucleons in nuclei A and B, 'y' is the rapidity in the centre-of-mass system of the collision and $F_A(y)$ is a contribution from a single wounded nucleon in A. Similarly, $F_B(y)$ is the contribution from a single wounded nucleon in B.

1.2.2 Participant-Spectator Model :

The Participant-Spectator model [11] of a heavy-ion collision is illustrated in Fig.1.2. The nuclei are Lorentz contracted along the direction of motion.

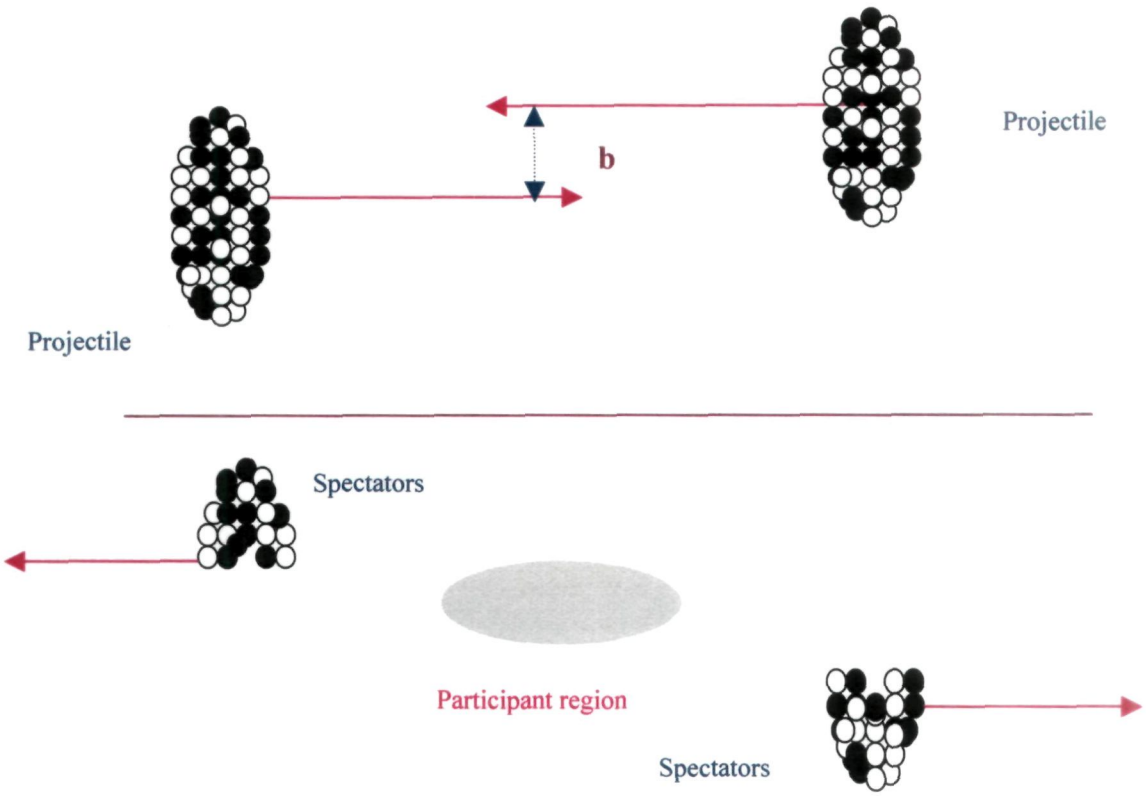

Fig 1.2 Participant-Spectator model for nucleus-nucleus collision

a) two Lorentz contracted nuclei before collision. Impact parameter 'b' determines the centrality,

b) after the collision, a participant region with high temperature and density is created.

The transverse distance beween the centres of the two colliding nuclei is called the impact parameter, denoted by symbol 'b'. For a given impact parameter, only the nucleons in the overlap region of the nuclei participate in the collision. These nucleons are usually called participants, the rest that do not participate in the collision are called spectators. For a head on collision, b=0 and the number of participants N_{part} will just be 2A in the hard sphere limit for an A+A collision.

The participating nucleons from overlapping nuclear parts create a volume of high temperature and density, while the spectators move basically undisturbed through the collision.To determine the collision geometry, measurements of quantities, which are strongly correlated to the number of participants, are used, such as transvese and forward energies and the no. of produced particles.

1.2.3 Hydro-dynamical Model :

This model was originally proposed by Landau [12] for explaining the multiparticle production phenomena in high energy hadronic collisions. Since then the model has been developed progressively as acceleator data at higher and higher energies became available. This model envisages collision of two Lorentz contracted nuclei (in the centre-of-mass frame) leading to formation of 'hot and dense' matter, which is assumed to be in local thermal equilibrium. Appropriate initial conditions in terms of distribution of fluid velocity and ther-

modynamical quantities are specified and then this 'hot and dense' matter follows hydrodynamical expansion, described by the conservation of energy-momentum, baryon number and other conserved numbers.

$$d_\nu T^{\mu\nu} = 0, \tag{4}$$

$$d_\mu (n_b u^\mu) = 0, \tag{5}$$

$$\ldots\ldots\ldots, \tag{6}$$

$$where \quad T^{\mu\nu} = (\epsilon + p) u^\mu u^\nu - p g^{\mu\nu} \tag{7}$$

is the energy-momentum tensor. n_B, n_s, ϵ, p are respectively the baryon number density, the strangeness density, the energy density and the pressure (specified in the proper frame of reference of the fluid element) and u^ν is the four-velocity of the fluid. Depending on the nature of the matter produced, some equation of state (Eos) is specified.

As the expansion proceeds, the fluid becomes cooler and cooler and more rarefied, until the constituent particles interact no more and are decoupled. The observable quantities such as $\frac{dN}{dy}$, $\frac{d\sigma}{d\eta}$ are then computed by using these decoupled or free particles.

References:

1. H.Satz, Nuclear Physics A715 (2003).

2. E. Witten, Phys.Rev., D36, (1984) 272.

3. I. Bombaci, Astronomy and Astrophysics, 305, (1996) 871.

4. H. Liu and G.L.Shaw, Phy.Rev., D30, (1984) 1137.

5. C.Griener, H.Stocker, Phys.Rev.Lett., 58, (1987) 1109.

6. C.Griener, H.Stocker, Phys.Rev., D44, (1991) 1109.

7. H.J.Crawford, M.S.Desai and G.L.Shaw, Phy.Rev., D45, (1992) 857.

8. Yves Schutz, J. of Physics G : Nucl. and Part.physics.,30 (2004) S903-909.

9. W. Busza, Acta Phys. Pol. B 8, 33 (1977).

10. A.Bialas and W.Czyz ; arXiV: hep-ph/0410265v1 19 oct 2004. ?

11. Fu-Hu Liu et al., Chinese J. Of phy. Vol 42, No.2 April2004.

12. L.D.Landau.,"Collectd papers of L.D.Landau" Pergamon Oxford, (1965) 569-665.

CHAPTER II

Experimental Techniques

2.1 Introduction :

Multiparticle production is an important phenomenon in high energy nucleus-nucleus collisions. Various parameters relating to emission characteristics of secondary particles like space localization of the trajectories of charged particles, emission angles, momenta of secondary particles, etc., are of immense importance in studying the mechanism of multiparticle production in these collisions.

Emission characteristics of particles produced in high energy hadron-nucleus (h-A) and nucleus-nucleus (A-A) collisions have been extensively studied using nuclear emulsion technique. As is well known nuclear emulsions serve as a detector as well as target and provide a good two-dimensional resolution; nuclear emulsions have high stopping power, which is about 1700 times more than that of the standard air [1]. Nuclear emulsions also provide 4 π angular coverage which makes them quite unique and suitable for investigating general features of nuclear interactions like multiplicity distribution, pseudorapidity distribution, cross-section, etc. Despite several advantages, nuclear emulsions have some disadvantages also like limited storage, non-linear response , dead-time at the beginning of an exposure, etc.

2.2 Composition of nuclear emulsions :

A photographic emulsion is essentially a dispersion of silver halide crystals in a gelatine matrix. ILFORD nuclear emulsions are fundamentally the same as general purpose photographic emulsions, but have the following several distinguishing features as well :

i) Silver halide crystals are very uniform in size and sensitivity and

ii) silver to gelatine ratio is much higher than in a conventional matrix.

Gelatine, which provides a three-dimensional network to locate crystals, is composed of Carbon, Nitrogen, Oxygen and Hydrogen together with glycerine. Glycerine is efficient to reduce the brittleness of the emulsion and the moisture in the emulsion prevents it from peeling off. A typical emulsion is composed [2-4] of : 1% hydrogen(H), 16% Carbon-Nitrogen-Oxygen(CNO) and 83 % silver-bromide(AgBr). The expression $< A > = \frac{\sum N_i A_i}{\sum N_i}$; can be used to calculate the average mass numbers of different groups of nuclei. The values of $\langle A \rangle$ for H,CNO, emulsion and AgBr groups of nuclei thus turn out to be equal to 1, 14, 74 and 94 respectively.

Table2.1

Composition of the standard nuclear emulsion

Element	Atomic number(Z)	Mass number(A)	Density gm/cm^3	No. of atoms/cm^3 ($\times 10^{22}$)
H	1	1	0.05	3.22
C	6	12	0.28	1.39
N	7	14	0.07	0.32
O	8	16	0.25	0.94
S	16	32	0.01	0.01
Br	35	80	1.34	1.01
Ag	47	108	1.83	1.02

2.3 Track formation

Bethe-Bloch formula[7] gives the mean rate of energy loss,(-dE/dx), by a charged particle while traversing through a medium :

$$-\frac{\mathrm{d}E}{\mathrm{d}X} = (\frac{4\pi \mathrm{N} Z z^2 e^4}{\mathrm{m}v^2 A})[ln(\frac{2mv^2}{\mathrm{I}(1-\beta^2)}) - \beta^2] \qquad (1)$$

where Z and A are respectively the atomic and mass numbers of the target atom, ze is the charge of the particle moving with a relative velocity β(=v/c), c being the speed of light in free space, N denotes the Avogadro's number, m is the rest mass of electron and I represents the mean ionization potential of the target atoms.

When an emulsion is exposed to an ionising radiation, clusters of silver

atoms are produced. These are known as latent image centres, as they are not visible until the emulsion is developed, when all the crystals containing a latent image centre are reduced to metallic silver, which appear black. The track of a charged particle, thus may appear as a series of black grains. When developing ILFORD nuclear emulsions, a developer is usually chosen which reduces those crystals containing a latent image centre completely and leaves those not containing a centre unchanged. All the residual silver halide is removed by fixation, leaving the metallic silver to form the image. If the silver halide was left in the emulsion, it would slowly go brown and degrade the image.

Information regarding the nature and velocity of the particle producing the track can be determined by studying the characteristics of a track. Generally, particles moving with higher velocities may ionize weakly and hence the grains formed will be quite rarer.

2.4 Ionization measurements

Though there are various methods to determine the ionization caused by charged particles while travelling through a medium, every method has certain limitations and is not efficient enough for measuring ionization caused by all types of charged particles. Some of the methods employed for measuring the ionization caused by charged particles are discussed below :

(i) Grain density method

This method is used for identifying the tracks produced by relatively faster particles. The number of developed grains per unit length of a track is known as grain density of a track. Specific ionization, $g^* = (\frac{g}{g_o})$; where g is the grain density of any track and g_o is the corresponding grain density of the primary

track, is a very good parameter for estimating the ionization produced by a charged particle.

(ii) Blob and gap method

This method is quite suitable for measuring ionization produced by a charged particle having comparatively smaller velocity. A slower charged particle produces relatively more ionization and consequently, grains are formed close together and exact counting of the grains becomes quite difficult. Blob and gap method is based on the observation of O' Ceallaigh[7], that the gap-length distribution follows exponential behaviour as:

$$H(l) = Be^{(-gl)} \tag{2}$$

where H(l) denotes the density of the gaps having lengths greater than a certain length l and B represents the blob density. It may be noted that the gap length, l, is chosen in such a manner that the number of blobs is roughly four times the number of holes. Hence, by counting the numbers of holes and blobs, the value of g is calculated using Eq. 2.

(iii) Delta-ray counting

While traversing a nuclear medium, if the energy transferred by a charged particle to an atomic electron is very large, a series of short tracks appear branching from the main track.These short tracks having length greater than a certain minimum length are known as delta-rays [7-8]. This phenomenon may be attributed to the ionization producecd due to the secondary charged particles. Generally, the grain configuration to be counted as a δ-ray must attain a minimum displacement of 1.58μ from the axis of the main track.

2.5 Data Analysis

The Data was collected using Ilford G5 emulsion stacks exposed to the 14.5A Gev ^{28}Si beam from the Alternating Gradient Synchrotron (AGS) at Brookhaven National Labvoratory (BNL). NIKON microscope with 40X objective and a 10X eyepiece was used to scan the plates. Each Plate was scanned by two independent observers to increase the scanning efficiency. The final measurements were performed using an oil-immersion 100X objective.

After scanning ,the events were chosen according to the following criteria :

i) to ensure that the events considered are due to the real projectile beam, the incident beam track should not exceed more than 2^o from the main beam direction in the pellicle.

ii) events lying within 20μm from the top and bottom surface of the pellicle were rejected. This was done to reduce the error in the angle measurements.

iii) To ensure that the sample of events finally selected were due to genuine beam primaries and were not contaminated with the secondary interactions due to particles/fragments produced in some other interactions in the same pellicle, all the primary tracks were followed back.

All the tracks produced by charged secondaries in these events were classified using emulsion terminology into the following groups :

i) Black Tracks (n_b) :

Tracks produced by particles with specific ionization $g^*>10$ ($g^* = g/g_0$),where g_0 is the plateau ionization of a relativistic singly charged particle.This corresponds to protons of relative velocity $\beta < 0.3$ and range in emulsion L < 3.00 mm .

ii) Grey Tracks (n_g) :

Tracks with specific ionization $1.4 \leq g^* \leq 10$ corresponding to protons having velocity in the interval $0.3 \leq \beta \leq 0.7$ and range $L \geq 3.0$ mm in nuclear emulsion. The black and grey tracks taken together in an event are known as heavily ionizing tracks $n_h = n_b + n_g$.

iii)Shower Tracks (n_s) :

Tracks with specific ionizations $g^* < 1.4$ which corresponds to particles having relative velocities $\beta > 0.7$ are reffered to as shower tracks. These tracks are mostly due to pi-mesons with small admixture of charged kaons and relativley faster protons.

The sum of the number of shower and grey tracks in an interaction is known as compound particle multiplicity and thier number in a collision is denoted by $n_c = n_g + n_s$

The exact identification of target in emulsion experiment is not possible since the medium is composed of a mixture of H,C,N,O,Ag and Br nuclei. To ensure that the targets in the emulsion are silver or bromine nuclei , we choose only the events with at least eight heavily ionizing tracks of (black + grey) particles, that is $n_h \geq 8$. The events which have the number of heavy tracks less than eight are due to the collision of the projectile beam with Carbon, Nitrogen and Oxygen nuclei present in the emulsion. These types of events are due to CNO nuclei.

2.6 Angular measurements

By determining the space angle of a track with respect to the primary, the angle of emission of a particle is determined. To get the space angle of a track

with respect to the mean direction of the primary, its projected angle in XY plane and dip angle in YZ plane are determined directly. Once the projected angle, θ_p,and the dip angle , θ_d, are known the space angle is calculated from

$$\theta_s = cos^{-1}[cos\theta_p * cos\theta_d] \tag{3}$$

However, it is very difficult to measure the angles directly if the angular seperation of a track is very small. In such cases, X, Y and Z co-ordinates at two points on the track are measured and θ_p and θ_d are calculated using the following expressions:

$$\theta_p = tan^{-1}\left(\frac{dY}{dX}\right) \tag{4}$$

$$\theta_d = tan^{-1}\left(\frac{dZ}{dX}\right) \tag{5}$$

It should be noted that the dip angle, θ_d, in the unprocessed emulsion is calculated from:

$$\theta_d = tan^{-1}\left(\frac{SF * dZ}{dX}\right) \tag{6}$$

where S.F. is the shrinkage factor, which is the ratio of the thicknesses of the unprocessed and the processed emulsion. The space angles of the tracks having smaller angular separations are calculated[1] using

$$\theta_s = cos^{-1}\left[cos\left(tan^{-1}\left(\frac{dY}{dX}\right)\right) * cos\left(tan^{-1}\left(\frac{SF * dZ}{dX}\right)\right)\right] \tag{7}$$

References:

1. M. S. Khan : Ph.D. Thesis submitted to Jamia Milia Ialamia Univ. New Delhi, India, (1993).

2. C.F.Powell, P.H.Fowler and D.H.Perkins : The study of elementary particles by photographic method, Pergammon Press London, (1959).

3. David M. Ritson, Techniques of High Energy Physics, Interscience Publishers,Inc., New York, (1961) 165.

4. W.H.Barkas : Nuclear Research Emulsions, Vol I, New York Academic Press, (1963);Nuovo Cimento.,(1958)201.

5. S.Garpman et al : Instrumentation method, A269, (1988) 134..

6. D.H.Perkins : Introduction to High Energy Physics 4^{th}edition, Cambridge University Press (2000) 349.

7. C.O'Ceallaigh : Nuovo Cimento.,12, (1954) 412.

CHAPTER III
General characteristics.

3.1 Introduction

Study of relativistic nucleus-nucleus collisions offers unique possibility to investigate the characteistics of hadronic matter at extreme values of temperature and densities . At energy densities above a few GeV fm^{-3}, hadrons in the reaction zone are visualized not to exist as discrete entities; they are believed to dissolve into a plasma of quarks and gluons [1-2].

Nuclear collisions are complex multibody reactions in which three stages may be identified: i) the interpenetration of the nuclei with highly non-equilibrium hadronic - and at high energies partonic interactions ; ii) the 'burning' of the fireball with its evolution towards chemical and thermal equilibrium ; iii) the 'freeze out ' of the final state hadrons. There are various experimental observables which give access to the physics of a nuclear collision[3]. For investigating the salient features of the de-confined state of nuclear matter, QGP, a thorough study of the global observables such as deposition of energy, momenta spectra and multiplicity distribution of secondary particles is expected to play a crucial role in understanding the mecha-

nisms involved[4-6]. In the present section, some important characteristics of the produced particles such as mean multiplicities, multiplicity distribution, pseudorapidity distribution and correlation among the secondary produced particles in 14.5 A GeV/c ^{28}Si-nucleus interactions are presented. For comparing the experimental results of the present study with the corresponding results determined for the data generated using Lund Model, FRITIOF, are also presented.

3.2 Particle Multiplicity & Multiplicity Distribution

Particle multipllicity as a global observable is one of the most general characteristics of the nucleus-nucleus collisions and gives important information about : i) how initial energy available is distributed for producing particles in the final state, ii) centrality of the collision and iii) underlying dynamics of the particle production mechanism.

Multiplicity is regarded to be one of the most important parameters for studying multiparticle production mechanism and with a knowledge about its behaviour, different phenomenological and theoretical models can be tested and modified. Mean multiplicities of various types of charged secondaries produced in 14.5A GeV/c ^{28}Si-nucleus interactions are listed in Table 3.1 and the values for ^{28}Si-nucleus and ^{12}C-nucleus collisions at 4.5A GeV/c [7-

8] are given in Table 3.2. It may be of interest to mention that $\langle n_b \rangle$, $\langle n_g \rangle$ and $\langle n_s \rangle$ are observed to vary with the projectile mass, A_p, as: $\langle n_x \rangle \propto {A_p}^{\alpha_x}$, where x = b, g, s, $\langle n_x \rangle$ denotes the corresponding mean multiplicity and α_x is a constant to be determined using the relevant data. The values of α_x are found to be $\alpha_b = 0.72 \pm 0.10$, $\alpha_g = 0.67 \pm 0.09$ and $\alpha_s = 0.18 \pm 0.08$. From Tables 3.1 and 3.2, the mean multiplicity of relativistic charged particles, $\langle n_s \rangle$, is found to increase rapidly with the projectile mass which is compatible with the predictions of the superposition models[9-10].

From these tables it is seen that the value of the mean multiplicity of relativistic charged particles, $\langle n_s \rangle$, increases with increasing projectile energy. The mean multiplicity of grey particles, $\langle n_g \rangle$, also shows an increasing trend with increasing mass as well as energy of the projectile. However, the mean multiplicity of black tracks, $\langle n_b \rangle$, does not exhibit any particular trend. On the other hand, the value of the mean multiplicity of charged particles, $\langle n_c \rangle$ is observed to increase with increasing mass as well as energy of the projectile. In Table 3.1 the values of $\langle n_b \rangle$, $\langle n_g \rangle$, $\langle n_s \rangle$ and $\langle n_h \rangle$ for the FRITIOF data are also presented.

Multiplicity distributions give a deeper insight into the dynamics of the high energy nuclear interactions and the particle production process. Possi-

Table3.1

Mean multiplicities of various charged particles for the experimental and FRITIOF generated data on 14.5 A GeV/c ^{28}Si-nucleus collisions.

	Experimental			FRITIOF		
	CNO	Em	AgBr	CNO	Em	AgBr
$\langle n_b \rangle$	2.84±0.11	6.96±0.22	10.50±0.24	1.92±.03	1.91±.03	3.72±0.10
$\langle n_g \rangle$	1.77±0.08	4.65±0.17	7.15±0.23	1.81±.04	2.71±0.05	8.24±0.10
$\langle n_s \rangle$	16.33±0.63	21.32±12.90	26.25±0.86	19.81±0.44	23.58±0.41	56.68±0.90
$\langle n_h \rangle$	2.27±0.63	5.23±0.85	8.15±1.13	3.73±0.04	4.63±0.07	11.95±0.18
$\langle n_{ch} \rangle$	18.15±0.64	26.72±0.72	17.64±0.40	21.62±0.46	26.30±0.45	64.93±0.89

Table3.2

Mean multiplicities of particles produced in ^{12}C-nucleus and ^{28}Si-nucleus collisions at 4.5 A GeV/c

	4.5GeV/c ^{12}C-beam			4.5GeV/c ^{28}Si-beam		
	CNO	Em	AgBr	CNO	Em	AgBr
$\langle n_b \rangle$	3.00±0.10	7.37±0.02	13.70±0.36	2.93±0.07	6.74±0.41	13.31±0.31
$\langle n_g \rangle$	1.57±0.07	5.51±0.21	5.94±0.24	1.53±0.06	3.72±0.22	7.38±0.02
$\langle n_s \rangle$	4.98±0.22	6.91±0.19	8.87±0.26	7.84±0.35	13.26±0.45	17.09±0.58
$\langle n_h \rangle$	9.55±0.76	19.78±0.51	28.76±0.61	12.30±0.36	24.85±0.62	37.79±0.95

bility of describing nucleus-nucleus (A-A) collisions as a superposition of h-h or h-A collisions may be investigaed by studying the multiplicity distributions of various classes of charged particles. Likewise , a detailed study of compound multiplicity, $n_c(=n_g+n_s)$ is expected to provide useful information regarding the particle production mechanism[7,12-17]. Multiplicity distributions of relativistic charged particles produced in ^{28}Si-nucleus collisions and compound multiplicity, $n_c(=n_g+n_s)$, are displayed in Fig 3.1. These distributions are described remarkably well by the negative binomial distribution (NBD)[4,11-12]. It has been seen that NBD is statistically equivalent to a combination of Poisson and logarithmic distributions. The NB distribution for n charged secondaries has two parameters, $\bar{n}$ and k, and energy dependence of the distribution is described by the energy dependent parameter k. The distribution is expressed as :

$$p(n,\overline{n},k) = k(k+1).....(k+n-1)\left(\frac{\frac{\overline{n}}{k}}{1+\frac{\overline{n}}{k}}\right)^{n}\left(\frac{1+\frac{\overline{n}}{k}}{n!}\right)^{k} \qquad (1)$$

where n and $\bar{n}$ represent respectively the multiplicity and mean multiplicity; the value of k is determined from

$$\frac{1}{k}+\frac{1}{\overline{n}} = \frac{D^2(n)}{\overline{n}} \qquad (2)$$

The physical process involved in the interaction mechanism can be explained

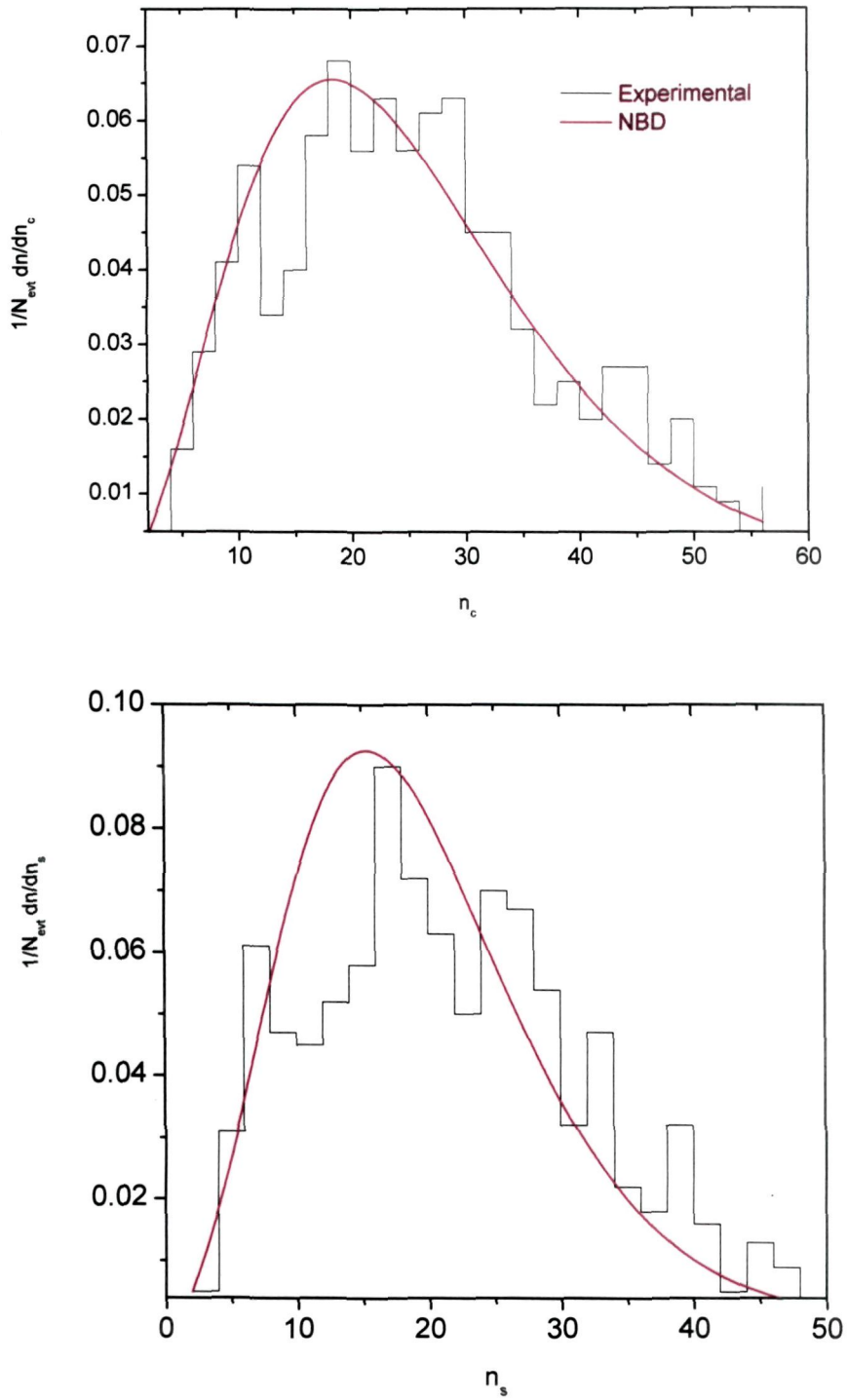

Fig. 3.1 n_s and n_c distributions for 14.5 A GeV/c ^{28}Si-nucleus interactions.

reasonably well by the cascade models[16-17]. It is further seen that the shapes of the distributions for the simulated data are nearly similar to those obtained for the experimental data. The estimated values of $\bar{n}$, k and χ^2/D.F. for the NBD fits, obtained using the CERN standard programme, MINUIT, are given in Table 3.3. The experimental values of $< n_s >$and $< n_c >$ are also presented in the same table. It is seen in the table that the values $< n_s >$ and $< n_c >$ for the collisions of ^{28}Si-nuclei with emulsion are reproduced very well by NBD.

Table3.3

Values of the parameters $\langle n \rangle$, k , χ^2/D.F for the Experimental data on 14.5A GeV ^{28}Si-emulsion.

Data type	n_s				n_c			
	$\langle n_s \rangle$	$\langle n_s \rangle_{est}$	k	χ^2	$\langle n_s \rangle$	$\langle n_s \rangle_{est}$	k	χ^2/D.F
EXP	21.32 ±0.90	19.56 ±1.24	5.10 ±0.55	0.79	23.10 ±0.56	24.95 ±1.09	3.76 ±0.25	0.46

3.3 Multiplicity correlations

Multiplicity correlations are of great significance in the study of multiparticle poduction in relativistic nuclear collisions. Several workers [9,12-13] have investigated the correlations of the type $\langle n_i(n_j)\rangle$, where i, j = b, g, s and h with i $\neq$ j, over a wide incident energy range involving different projectiles. In this section, an attempt is made to study multiplicity correlations amongst the secondary charged particles produced in 14.5A GeV/c ^{28}Si-emulsion interactions . Shown in Fig. 3.2 are the correlations of $\langle n_x\rangle$, x = b, g, c and h with n_s. The experimental results are analysed by using the least squares fitting of the type :$\langle n_i(n_j)\rangle = a_{ij} + b_{ij}n_j$. The values of the slope 'b' and intercept 'a' for various correlations are listed in Table 3.4. From Table 3.4 and Fig.3.2 it may be concluded that there is a linear dependence between the mean multiplicities of heavily ionizing particles and n_s. It can also be seen that $\langle n_h\rangle$ and $\langle n_c\rangle$ are individually quite strongly correlated with n_s in comparison to the correlations of $\langle n_b\rangle$ and $\langle n_g\rangle$ with n_s.

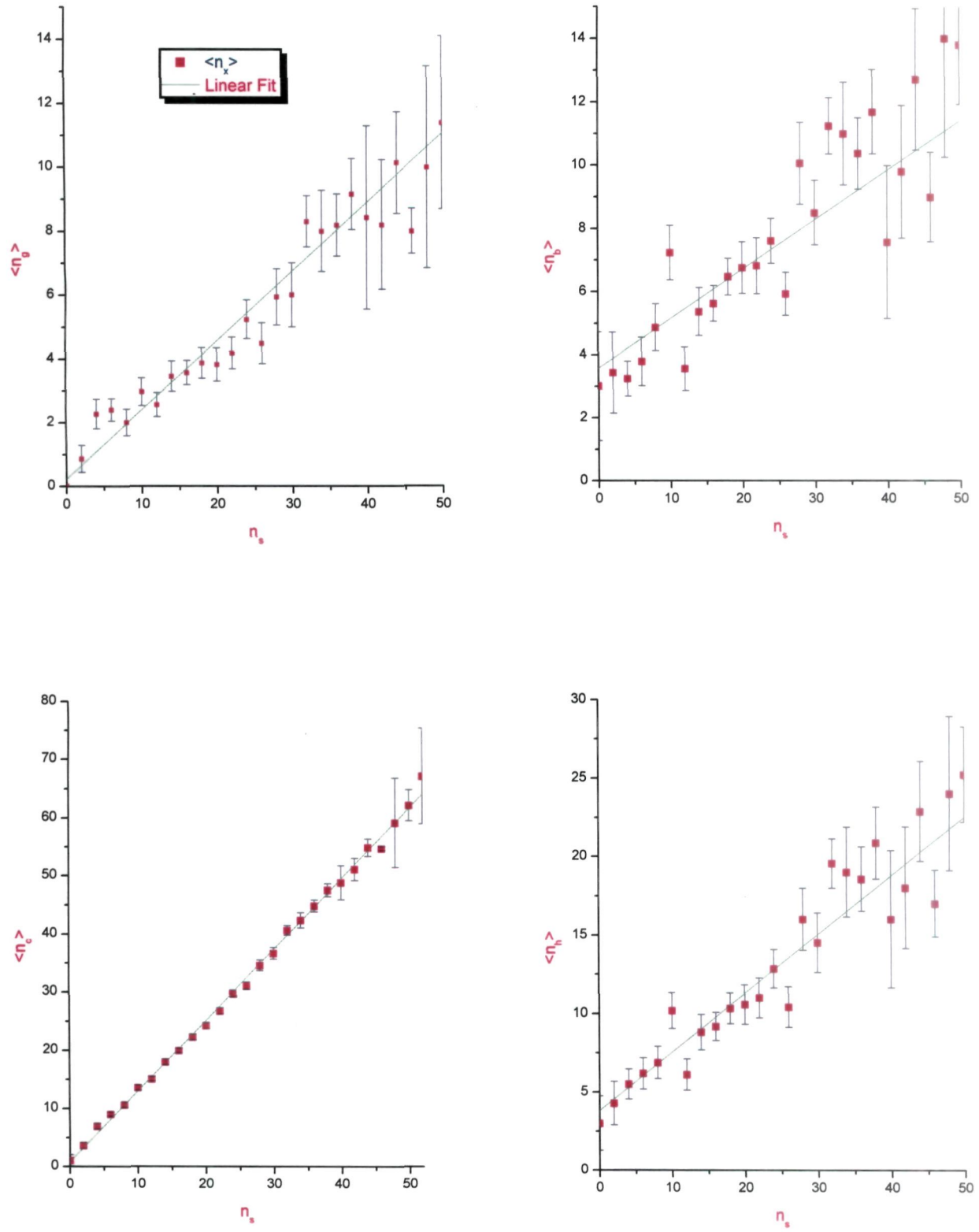

Fig.3.2 Variations of $\langle n_x \rangle$ (x=b,g,h and c) with n_s in 14.5A GeV/c ^{28}Si-emulsion interactions.

Table3.4

Values of a_{ij} and b_{ij} in the multiplicity correlations in Si-Em interactions at 14.5A GeV/c

	$\langle n_s \rangle$	
	a_{ij}	b_{ij}
$\langle n_g \rangle$	0.23±0.39	0.22±0.01
$\langle n_b \rangle$	3.57±0.88	0.52±0.03
$\langle n_c \rangle$	0.84±0.37	1.21±0.01
$\langle n_h \rangle$	3.80±0.85	0.37±0.03

3.4 Angular characteristics

3.4.1 Pseudorapidity distribution

Rapidity distribution allows us to address some important questions relating to reaction dynamics and the properties of particle-emitting source[3]. One uses rapidity distribution due to the reason that the shape of the distribution is Lorentz invariant.The rapidity of a particle, y, is defined as :

$$y = \frac{1}{2} ln(\frac{E + p_l}{E - p_l}) \qquad (3)$$

where E and p_l represent total energy and longitudinal momentum respectively

The rapidity of a particle in one frame of reference is related to rapidity in another moving Lorentz frame as:

$$y' = y - y_\beta \tag{4}$$

where y_β is the rapidity of the moving frame and is given by

$$y_\beta = \frac{1}{2} ln \frac{1+\beta}{1-\beta} \tag{5}$$

This simple property of rapidity variable makes it suitable to describe the dynamics of relativistic particles [1]. At high energies $p_l >> p_t >> m$, where m and p_t respectively denote the rest mass and transverse momentum of the secondary particle, the expression for rapidity reduces to, pseudorapidity, η :

$$\eta = -lntan(\frac{\theta}{2}) \tag{6}$$

where θ is the space angle of the secondary particle with respect to the mean direction of the incident particle . Experimentally, it is not always possible to measure the energy and momentum of a particle , hence , it is more convenient to use pseudorapidity variable, η.

Pseudorapidity distribution of the relativistic charged particles emitted

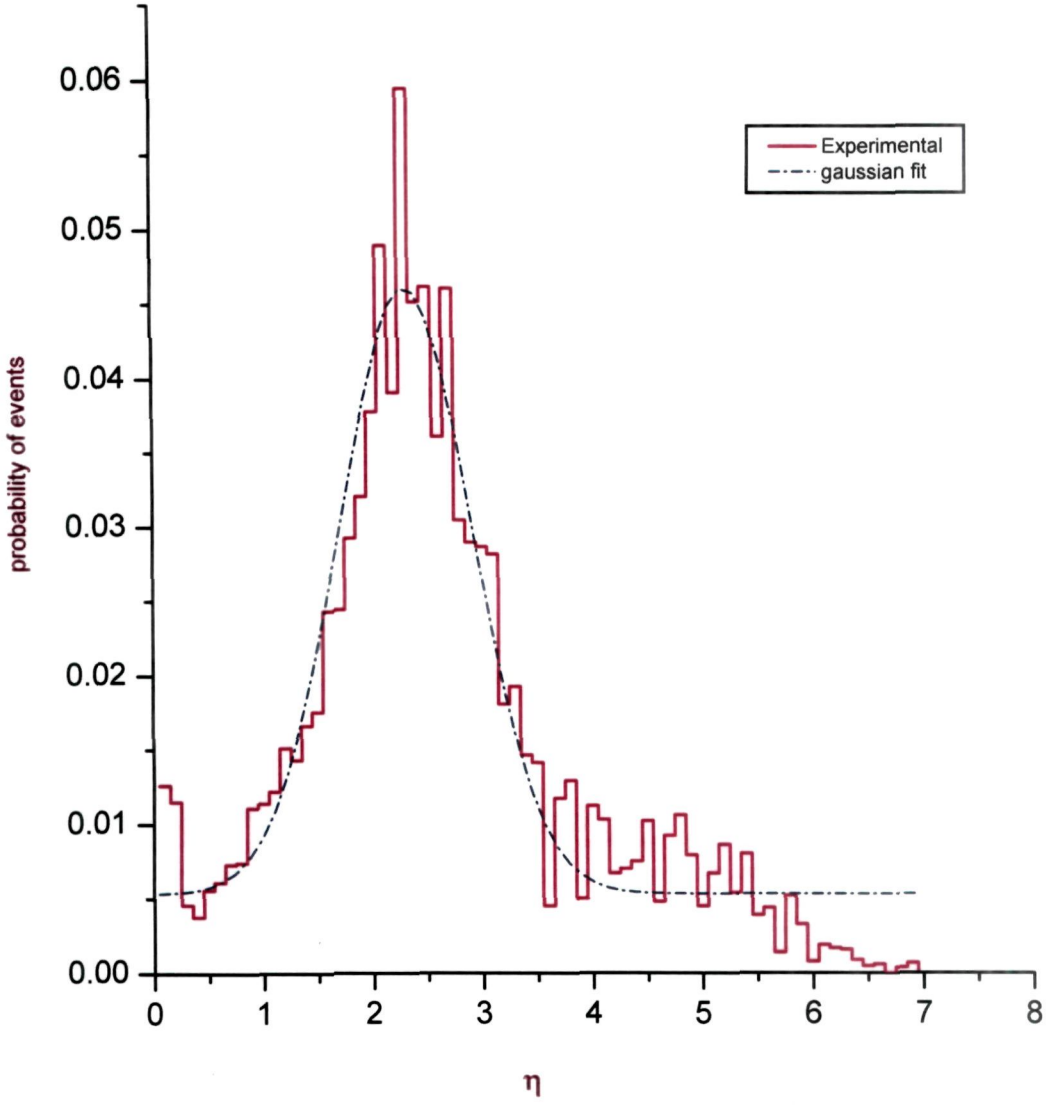

Fig.3.3 Pseudorapidity distribution of relativistic charged particles produced in 14.5 A GeV ^{28}Si-emulsion interactions.

in ^{28}Si-Em interactions at 14.5 A GeV/c is shown in Fig 3.3. As can be seen in the figure the distribution is nicely fitted by a gaussian distribution as predicted by various models [14].

In Fig 3.4, rapidity densities for different n_h-intervals are plotted to examine any target dependence. The distribution may be divided into three regions viz.,target fragmentation , projectile fragmentation and central /pionic regions.The target fragmentation region corresponds to smaller η -values, i.e., larger values of emission angles which is characterised by the target nuclei. The projectile fragmentation region envisaged to be populated by fragments of the projectile nucleus corresponds to larger values of η i.e. smaller angles of emission. The central region is believed to be populated by the particles produced in collision of participant region of the colliding nuclei and is independent of either fragmentation regions[15].

Dependence of various angular characteristics, namely, pseudorapidity, average pseudorapidity, rapidity dispersion,rapidity widths etc., of relativistic charged particles on n_s is investigated by dividing the experimental data into the following n_s intevals :

i) $n_s \leq 9$

ii) $10 \leq n_s \leq 20$

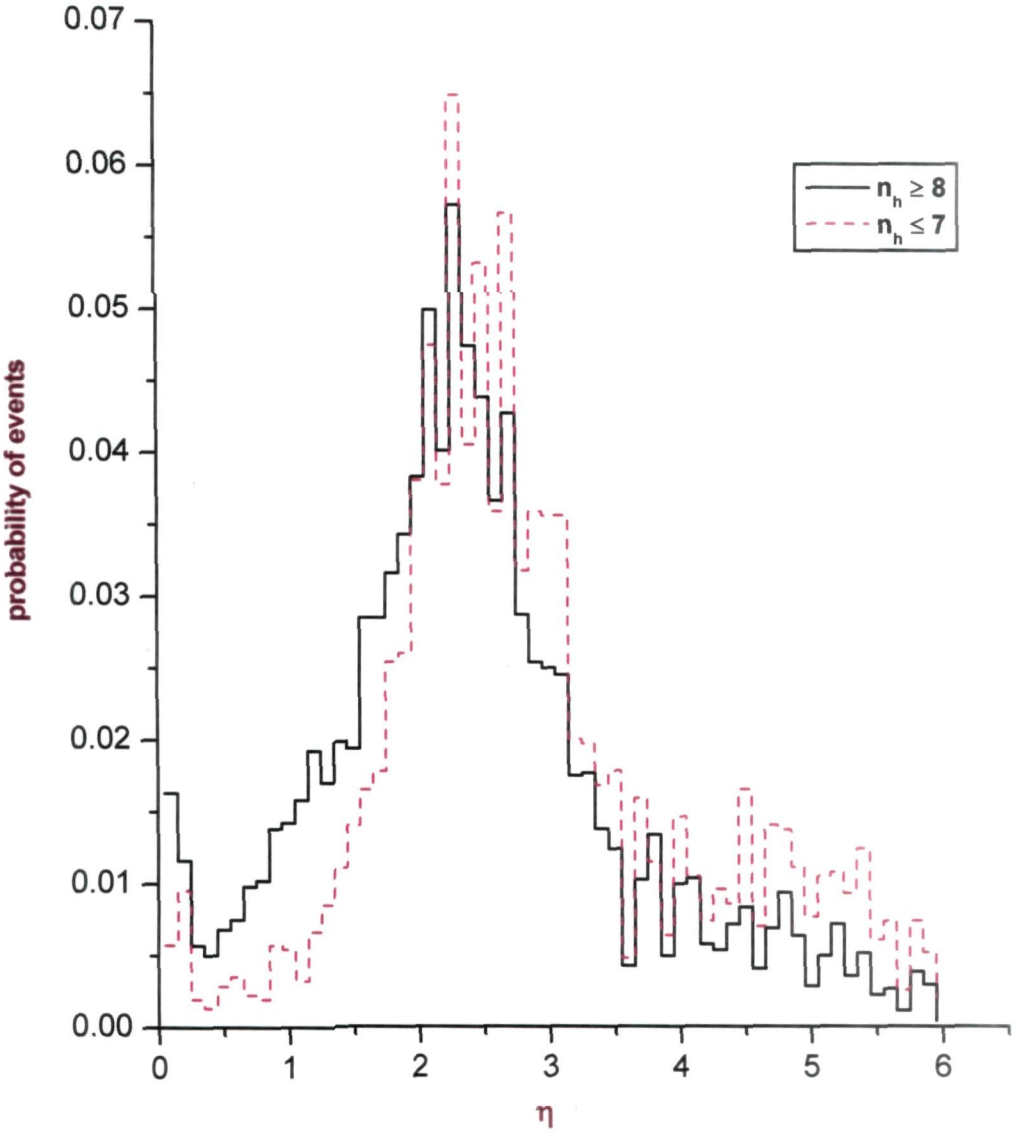

Fig 3.4 Pseudorapidity distributions of relativistic charged particles produced in 14.5 A GeV/c 28Si-Em collisions for i) $n_h \geq 8$ and ii) $n_h \leq 7$

iii) $n_s \geq 21$

η spectra of relativistic charged particles produced in 14.5 A GeV/c ^{28}Si - emulsion interactions for the above n_s bins are plotted in Fig 3.5. It may be seen that the trends of variation of η distributions remain almost similar at large as well as at small η values , whereas the distributions peak in the central part of the η spectrum. This would imply that the central part of η distribution is enriched with particles. This criterion can be used to define the central rapidity region. Several interesting features of particle production such as thermalisation and hadronization, etc., are expected to be inherent in the central region. Also, the particles produced within this rapidity interval are visualized to be free from the influence of fragmentation of both target and beam nuclei[16-18].

Average value of pseudorapidity, $\langle\eta\rangle$, for each collsion was determined by the following relation:

$$\langle\eta\rangle = 1/N\sum\eta_i \tag{7}$$

whre N represents the total number of particles produced in an interaction.

Distributions of $\langle\eta\rangle$ for the three categories of interactions are shown in Fig 3.6. It can be seen that the distribution shifts towards lower value of $\langle\eta\rangle$ with increasing n_s and the height of the peak also increases with increasing

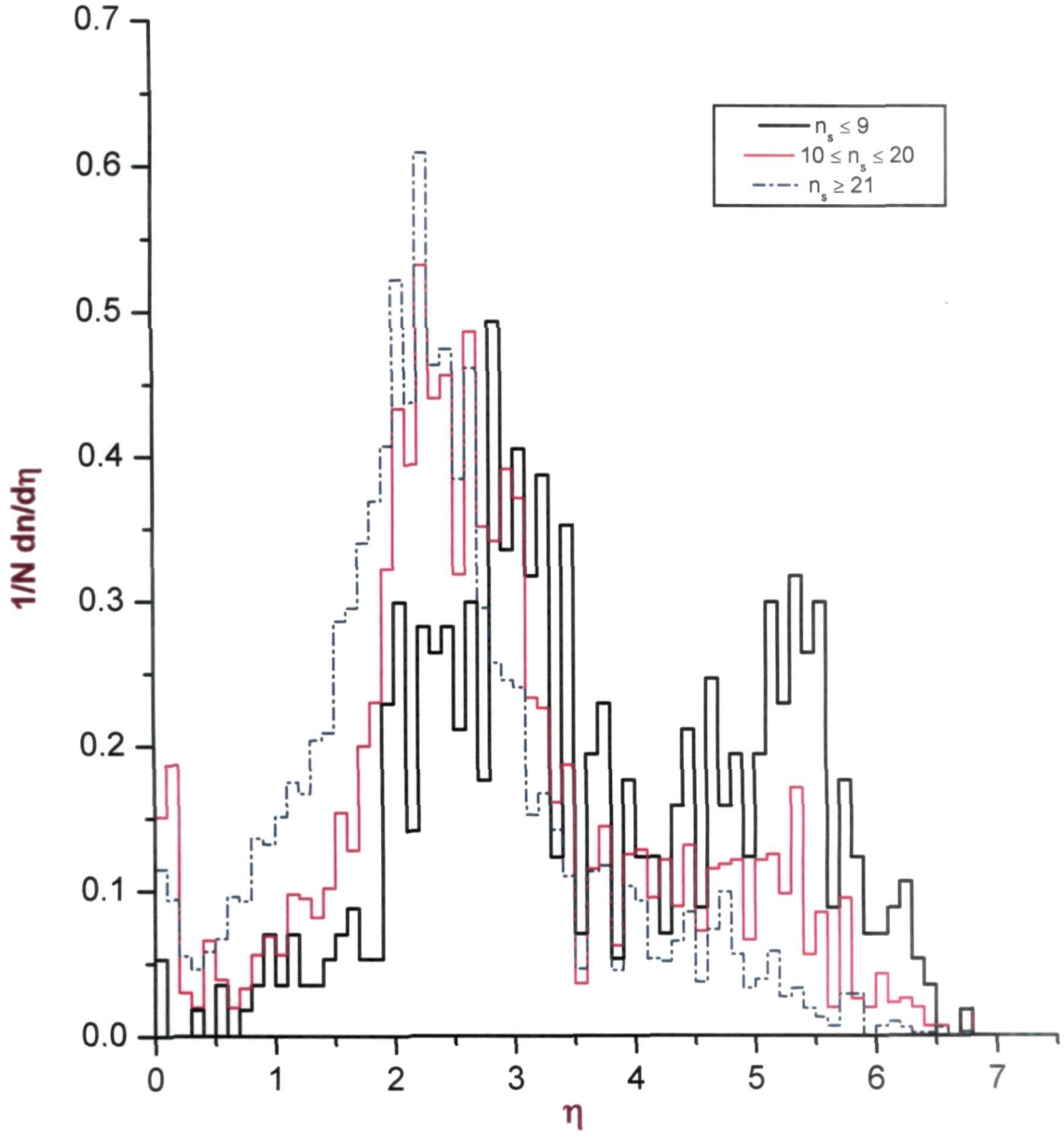

Fig3.5 Dependence of η-distribution for different n_s intervals

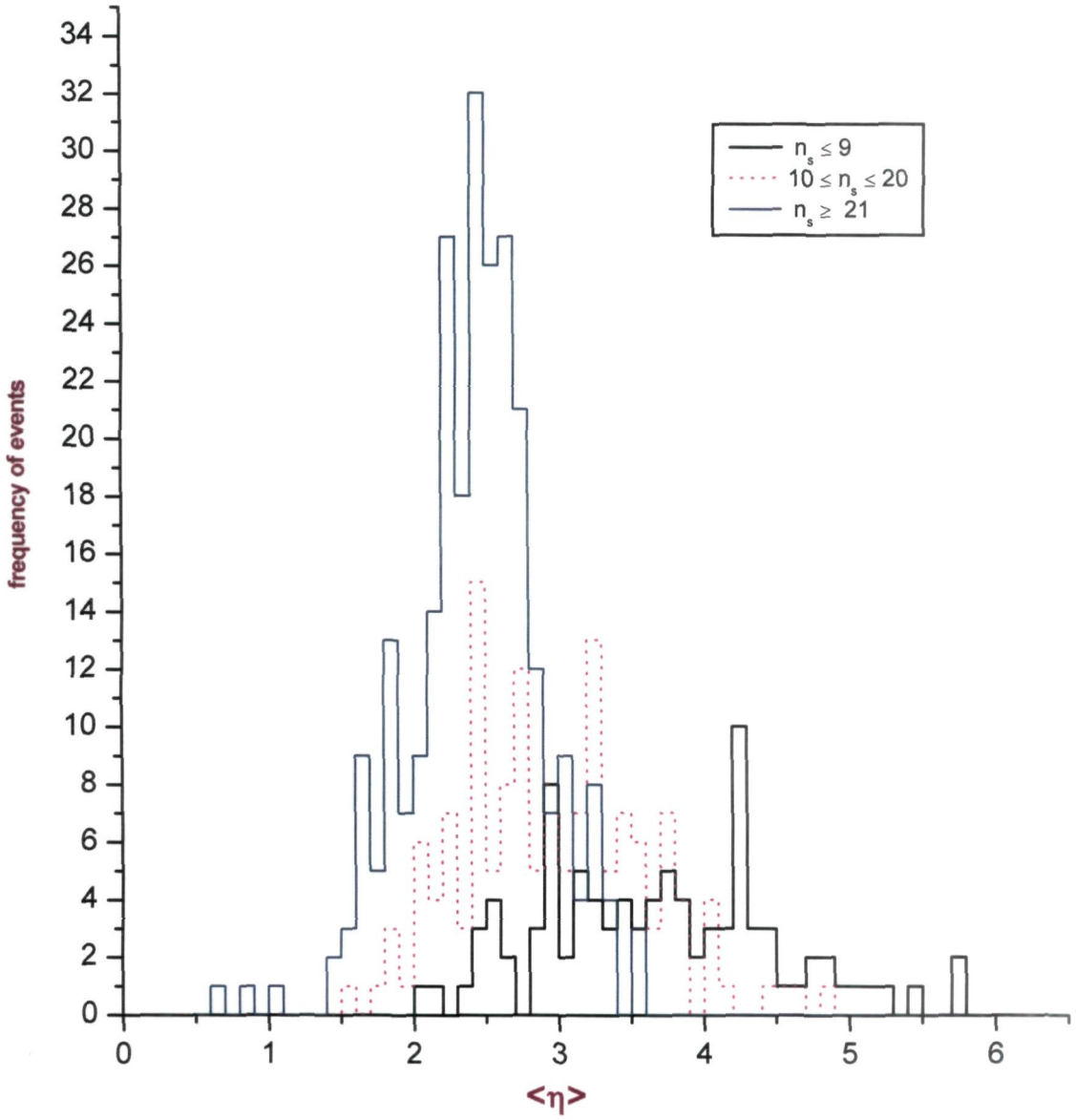

Fig 3.6 Distribution of $<\eta>$ in different n_s bins.

n_s. Also, the width of the distribution strongly depends on the multiplicity of relativistic charged particles[17-19].

3.4.2 D(η) distribution of relativistic charged particles

Event-by-event calculation of rapidity dispersion,D(η), can be used to measure the clustering of the particles produced along the longitudinal rapidity axis at higher energies [25-20]. The dispersion for each event is calculated using the following expression :

$$D(\eta) = [\langle \eta^2 \rangle - \langle \eta \rangle^2]^{\frac{1}{2}} \tag{8}$$

Fig 3.7 displays the D(η) distributions for the three classes of interactions characterized by : i) $n_s \leq 9$, ii) $10 \leq n_s \leq 20$ and iii) $n_s \geq 21$. As can be seen D(η) distributions remain essentially similar for the three groups of interactions but the height of the peak in the central D(η)region increases with increasing value of n_s. Also, discernible peaks are observed in the central part of the D(η) distributions, indicating thereby the occurrence of clusters[16-17].

For studying the dependence of the rapidity width R(η) on the multiplicity of the relativistic charged particles produced in 14.5AGeV/c ^{28}Si -

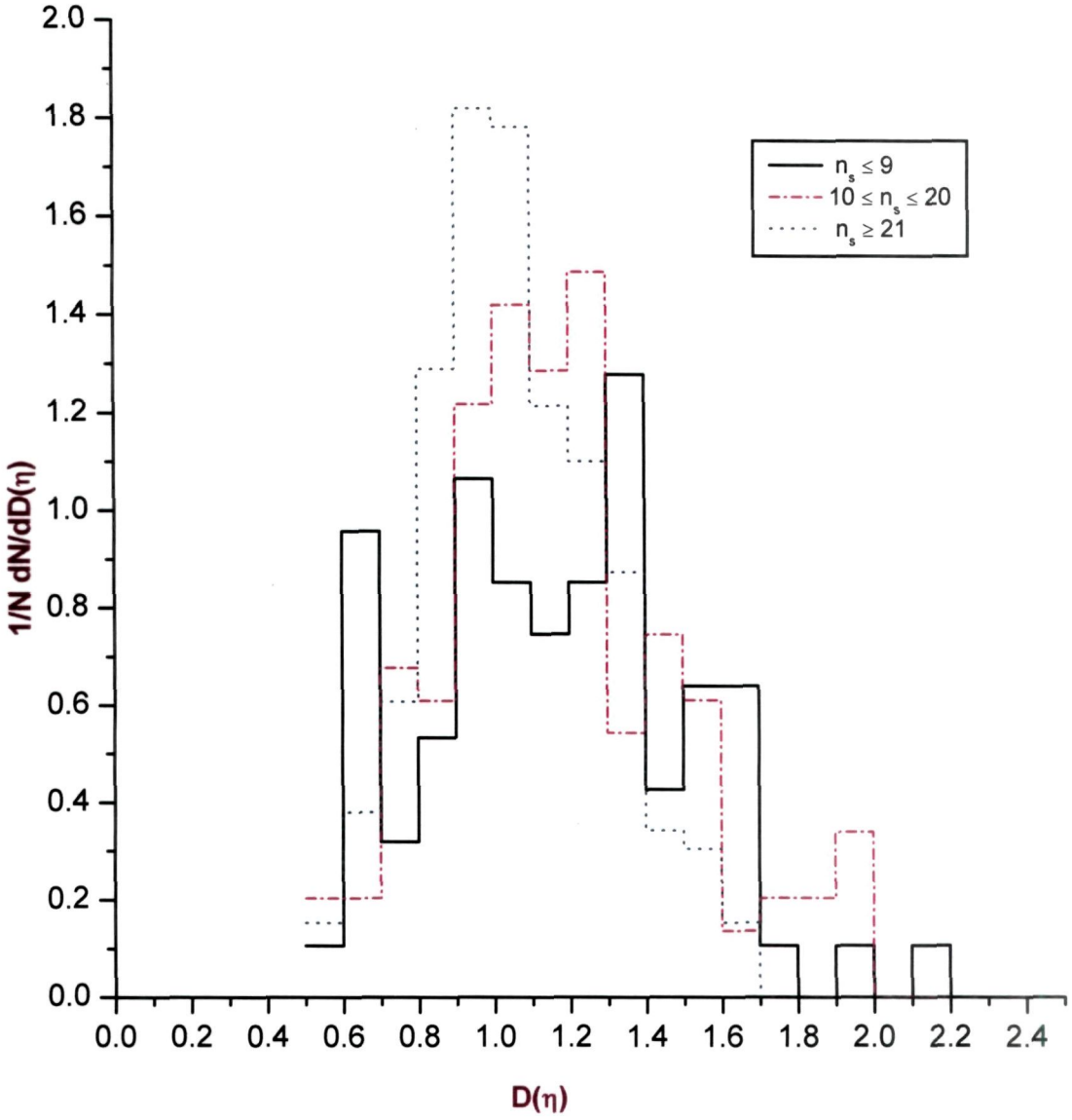

Fig 3.7 Distributions of dispersions of relativistic charged particles produced in in 14.5 A GeV ^{28}Si-emulsion interactions for different n_s intervals.

emulsion interactions the value of R(η),defined as :

$$R(\eta) = \eta_{max} - \eta_{min} \tag{9}$$

for each event is calculated. Fig 3.8 shows that R(η) distribution strongly depends on n_s and the peak of R(η) distribution is observed to shift towards higher values of R(η) with increasing multiplicity of relativistic charged particles[16-20].

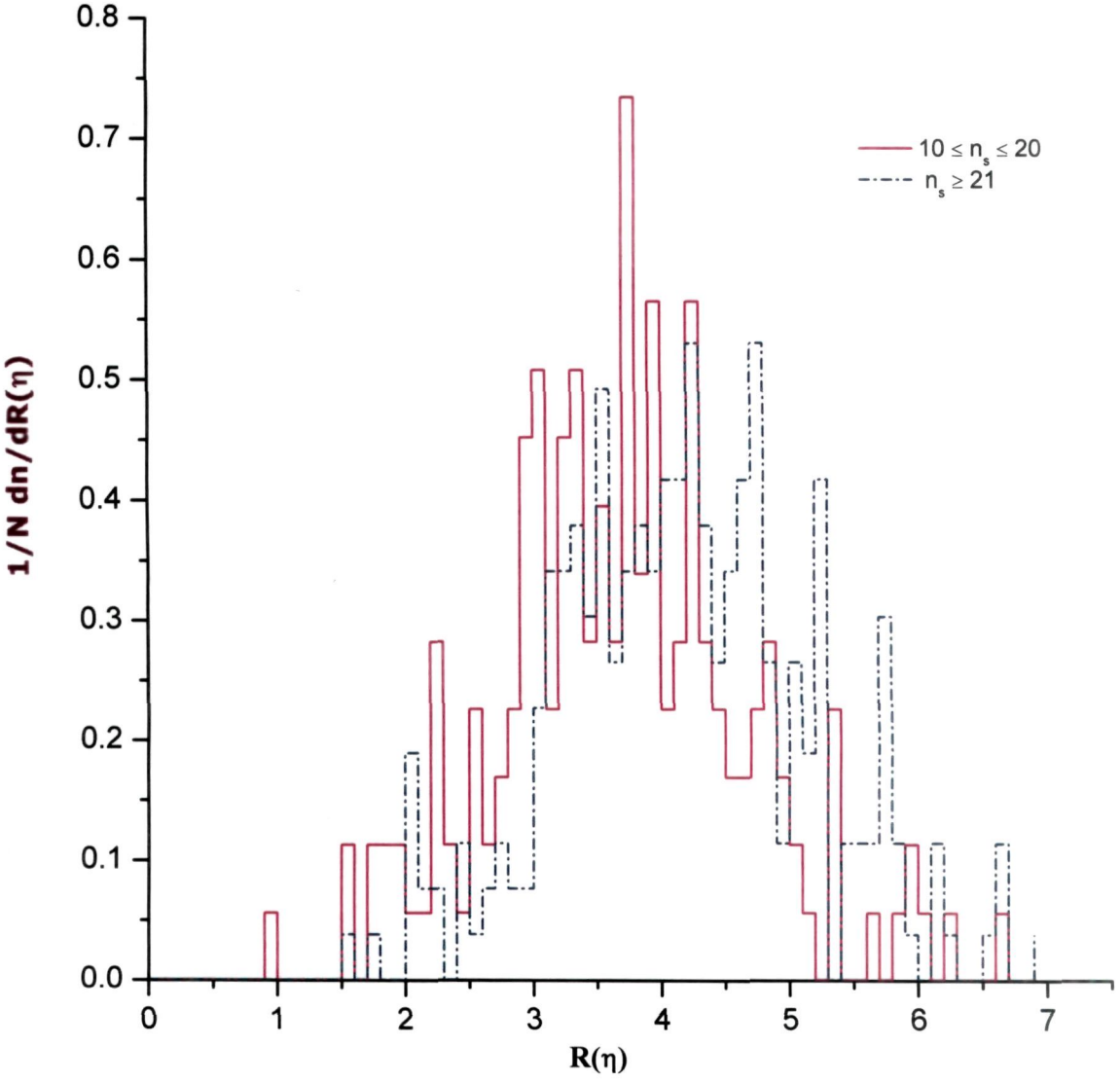

Fig3.8 Dependence of $R(\eta)$ on n_s.

References:

1. Cheuk -Yin Wong : Introduction to High-Energy Heavy Ion Collisions, World Scientific 1994.

2. H.R.Schmidt and J. Schukraft: J. Nucl. Part. Phys., G19, (1993) 1706; F.Becattini,J.Cleymans,A.Keranen,E.Suhonen and K.Redlich : Phys.Rev.,C64 (2001) .

3. Quark Matter 2002 ;proceedings of the 16th International Conference on ultra-relativistic Nucleus-Nucleus Collisions.,ELSEVIER

4. M. K. Hegab, M. T. Hussein and N. M. Hassan : J. Phys. **G16**, 615 (1990)

5. J. Boguta : Phys. Lett. **B109**, 251 (1982)

6. A. El. Naghy, N. N. Abd-Alla : Turkish J. Phys. **18**, 1106 (1994)

7. G. Singh et al : Phys. Rev. **C43**, 2417 (1991)

8. D. Ghosh et al: Nucl. Phys.**A499**, 815(1989)

9. Tauseef Ahmad and M.Irfan : Nuovo. Cim. **A106**, No.2, 171 (1993)

10. A. Capella and Y. Tran Than Yan : Phys. Lett. **B93**, 146 (1980)

11. Namrata, Ashutosh Bhardwaj, V.K. Verma et al., Eur.Physics J. A 13, 405-410 (2002).

12. M. Tariq, M. Zafar , A. Tufail and S. Ahmad : Int. J. Mod. Phys. **E4**, No. 2 , 347 (1995)

13. M.Saleem Khan, H.Khushnood, A.R.Ansari and Q.N.Usmani : Nuovo Cimento, No.2, (1995) 147.

14. M. I. Adamovich et. al.:EMU01 Collaboration, Z. Phys. **56** (1992) 520

15. M.Tariq, M.Zafar and S.Ahmad.,International J of Modern Physics E, vol.1 , No4(1992) ,859.

16. Nazeer Ahmad : *Ph.D. Thesis*, Aligarh Muslim University, Aligarh, India (2002)

17. M. Mohsin Khan:*Ph.D. Thesis*, Aligarh Muslim University, Aligarh, India(2005)

18. P.Singh,H.Khushnood: Int.J. Mod. Phy.,E7, No.6, (1998) 659

19. A.Shakeel,H.Khushnood, M.Irfan , A.Ahmad, A.H.Naqvi and M.Shafi : J. Phy. Soc. Jpn.,55,No.10,(1986)3362

20. A.Shakeel,W.B.Tak, N.Ahmad,A.R.Khan,M.Zafar,M.Irfan,A.Tufail and A.Ahmad : Int. J.. of Mod. Physics,E8, No.2,(1999)121.

CHAPTER IV

Study of Rapidity Gap Distribution and Correlations.

4.1 Introduction

Particle production in high energy hadronic and nuclear collisions has been extensively studied by many workers [4-10]. It has been envisaged that clusters may be formed during an intermediate stage of an interaction, which ultimately decay into real physical particles. Formation of clusters and thier sizes can be studied by examining the behaviour of rapidity differences between the n^{th} nearest neighbours [4-7].For this purpose, the values of pseudorapidities of all the relativistic charged particles in each event are determined and arranged in ascending or descending order leaving out the minimum and maximum values of rapidities for they are considered to constitute leading and target particles. Two-, three-, four- and five-particle rapidity differences are determined by calculating: $\eta_{i+1} - \eta_i$,$\eta_{i+2} - \eta_i$, $\eta_{i+3} - \eta_i$, and $\eta_{i+4} - \eta_i$, where i=1,2,3,....,..respectively.In this way n-particle correlations may be searched for by plotting the rapidity differences between the n^{th} nearest neighbours as histograms [4-5].

The characteristics of clusters is explained by studying rapidity gap distributions in terms of the predictions of Snider's model [1]. This model is essentially a two-channel generalization of the Chew-Pignotti multiperipheral model [2].It may be noted that Snider's model predicts the rapidity gap distribution to have the following form:

$$dn/dr = Aexp(-Br) + Cexp(-Dr) \quad (1)$$

where A, B, C and D are constants and 'r' is the rapidity difference between the n^{th} nearest neighbours; the values of parameters A, B, C and D have been predicted to have the values 2.40, 3.10, 0.20 and 0.90 respectively [1]. The first and the second terms in Eq.1 represent respectively the contribution of short- range and long-range correlations.The values of the slope parameters 'B' and 'D' are regarded to be the measures of cluster size and cluster density [1-5].An attempt is made to investigate correlations amongst relativistic charged particles as well as dependence of cluster size on i) the target mass and ii) multiplicity of relativistic sharged particles, n_s.

4.2 Dependence of cluster size on target mass

For examining the dependence of cluster size on target mass, rapidity gap distributions for two-, three-, four- and five-particles are analysed for the interactions due to CNO, AgBr and emulsion targets. Rapidity gap distri-

butions between two consecuetive particles for the interactions due to CNO, AgBr and emulsion targets are exhibited in Fig.4.1. It is clearly observed that the distributions peak at relatively smaller values of rapidity gaps, r , for all the three classes of intactions. Hence, it can be concluded that two-particle correlations exist in these interactions. Three-,four- and five-particle rapidity gap distributions for CNO, AgBr and emulsion targets are displayed in Figs 4.2, 4.3 and 4.4, respectively. It is seen that sharp peaks occur in the case of three- and four-particle rapidity gap distributions, however no such behaviour is observed in case of five-particle rapidity gap distribution.These observations, therefore, tend to suggest that, whereas two-, three- and four-particle correlations are present,five-particle correlation may not exist.Using Eq.1,best fits to the data are obtained and are shown by solid curves in each figure; these fits are obtained using CERN standard program MINUIT.The two broken lines in each figure represent the contributions of the two exponential terms individually appearing in Eq.1. From Figs 4.1-4.3, it can easily be inferred that the long-range contribution to two-, three- and four-particle correlations is quite negligible, whereas the short-range contribution is quite significant.

The values of parameters A, B, C and D appearing in Eq.4.1, obtained

for these distributions alongwith the corresponding values of $\chi^2/D.F.$ are listed in Table 4.1. As can be seen from the table, the value of the parameter 'B' remains essentially the same for the interactions due to CNO, AgBr and emulsion targets, that is, parameter 'B' is independent of the target mass. Moreover, the value of 'B' shows a decreasing trend with increasing cluster size. However, the value of parameter 'D' is almost unaffected by cluster size as well as target size.

Uncorrelated production of particles can be investigated by fitting five-particle rapidity gap distribution for the CNO, AgBr and emulsion targets with Wigner distribution [11], which is one of the nearest neighbours of the Gaussian Orthogonal Ensemble (GOE)-type distribution, represented by the expression :

$$P(x) = \pi/2x[exp(-\pi x^2/4)] \tag{2}$$

wher x = r/$\langle r \rangle$, $\langle r \rangle$ being the mean rapidity gap between the nearest neighbours for the entire events for a particular group of interactions considered in the present study. The absence of five-particle correlations is further substantiated by the fact that the five-particle rapidity gap distribution is reproduced reasonably well by the Wigner distribution.

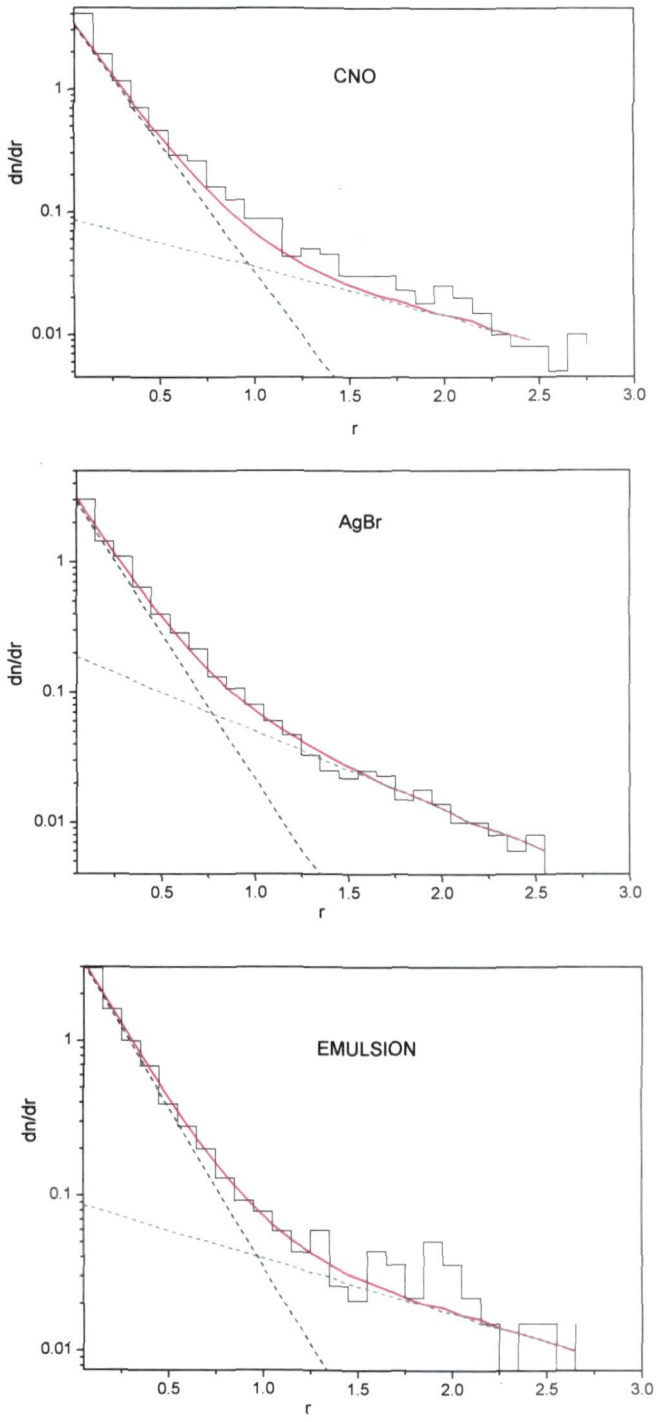

Fig.4.1 Two-particle rapidity gap distributions in 14.5A GeV/c ^{28}Si-nucleus interactions.

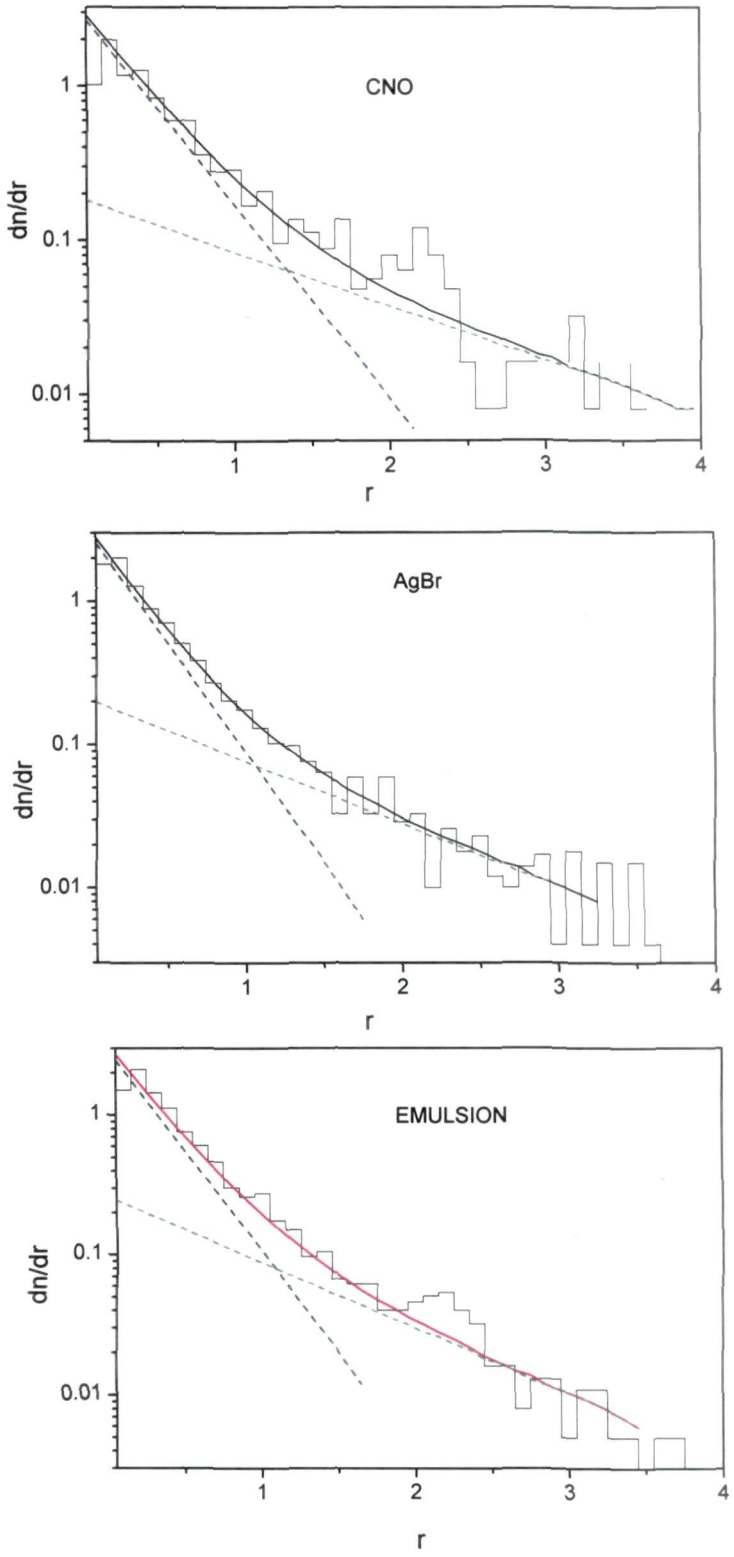

Fig.4.2 Three-particle rapidity gap distributions in 14.5A GeV/c ^{28}Si-nucleus interactions.

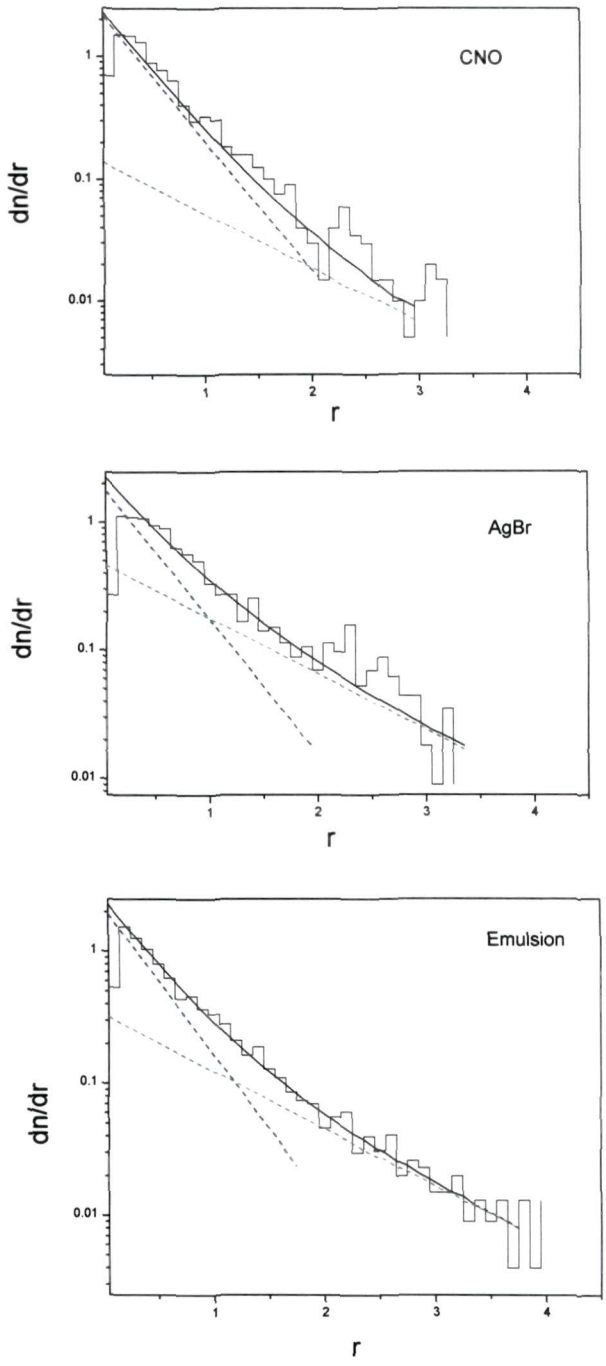

Fig. 4.3 Four-particle rapidity gap distributions for CNO, AgBr and emulsion targets in 14.5A GeV/c ^{28}Si-nucleus collisions.

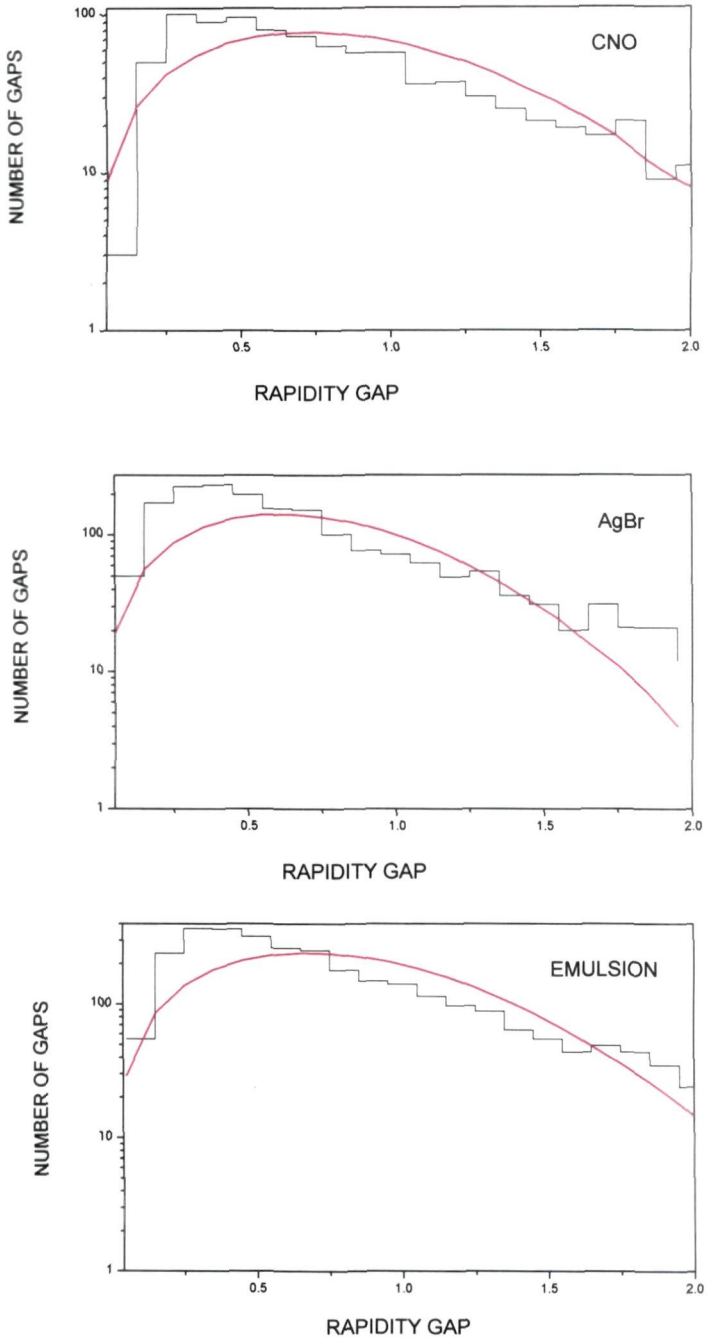

Fig. 4.4 Five-particle rapidity gap distributions for CNO, AgBr and emulsion targets in 14.5A GeV/c ^{28}Si-nucleus collisions. The curves in the figure represent the Wigner distribution.

Table4.1

Values of the parameters occurring in Eq.(4.1) obtained for 14.5A GeV/c ^{28}Si-nucleus interactions for different targets.

Cluster size	A	B	C	D	χ^2/D.F	χ^2/D.F (Wigner dist.)
Emulsion						
Two-particle	4.25±0.39	4.87±0.32	0.11±0.03	1.02±0.15	0.12	-
Three-particle	3.01±0.32	3.37±0.33	0.25±0.20	1.17±0.20	0.18	-
Four-particle	2.34±0.10	2.72±0.05	0.37±0.01	1.05±0.07	0.10	-
Five-particle	1.85±0.10	1.77±0.09	0.31±0.12	1.69±0.16	0.48	0.78
AgBr						
Two-particle	3.83±0.20	5.23±0.13	0.23±0.02	1.32±0.06	0.17	-
Three-particle	3.17±0.20	365±0.10	0.25±0.01	1.00±0.03	0.25	-
Four-particle	2.45±0.36	2.46±0.21	0.15±0.03	1.04±0.08	1.17	-
Five-particle	2.27±0.13	2.10±0.04	0.29±0.02	0.98±0.03	0.31	2.85
CNO						
Two-particle	4.02±0.29	4.83±0.20	0.09±0.01	0.85±0.10	0.20	-
Three-particle	3.13±0.20	2.98±0.10	0.21±0.01	0.80±0.03	0.52	-
Four-particle	2.10±0.27	2.54±0.20	0.51±0.30	1.00±0.04	0.28	-
Five-particle	2.93±0.20	2.30±0.04	0.29±0.04	0.57±0.10	0.24	0.17

4.3 Dependence of cluster size on n_s

In order to investigate the dependence of cluster size on relativistic charged particle multiplicity, the data on 14.5 A GeV/c ^{28}Si-nucleus interactions is divided into three groups on the basis of their n_s values : (i) $n_s \leq 9$, (ii) $10 \leq n_s \leq 20$ and (iii) $n_s \geq 21$.

Rapidity gap distributions for two adjacent particles and two alternate particles in different n_s-bins are exhibited in Figs 4.5 and 4.6, respectively. The distributions exhibit sharp peaks at relatively smaller values of rapidity gaps, r , and hence support the idea of occurence of two- and three-particle correlations. The solid curves in the figures represent best fits to the data obtained using Eq.1. The two broken lines represent the contributions due to the two terms in Eq.1. It is clear from the plots that in case of two- and three-particle rapidity gap distributions, the short range correlation plays a predominant role in comparison to the long range correlation.Four-particle rapidity gap distribution shown in Fig.4.7 does not exhibit any sharp peak in the case of interactions with $n_s \leq 9$. However, relatively sharper peaks occur in case of interacions with $n_s \geq 10$ for four-particle rapidity gap distributions.This observation would tend to suggest that four-particle correlation occur only in the interactions having $n_s \geq 10$.As can be seen from Fig.4.8,

no sharp and distinct peaks are observed in five-particle rapidity gap distributions for all the interactions lying in the three n_s intervals. Hence, it can be stated that five-particle correlation does not occur.

Using Eq.1, best fits to the data are obtained and are shown by solid curves in each figure. These fits are obtained using the CERN standard programme MINUIT.Values of these parameters together with χ^2/D.F. for each fit are given in Table 4.2. The value of parameter 'B', which is regarded as the strength of the correlation[1-2],is found to increase with increasing n_s. But it is observed to show a decreasing trend with increasing cluster size. However the value of 'D' does not show any definite trend for the three n_s-bins from which it can be concluded that the particles are produced independently, without any intermediate cluster being formed.This independent particle production contributes to the rapidity gap distributions at higher values of rapidity gaps.

Uncorrelated production of particles in different n_s-bins can be examined by comparing the five-particle rapidity gap distributions with the Wigner distribution. Also, four-particle rapidity gap distribution for the interactions with $n_s \leq 9$ is compared with the Wigner distribution Fig 4.7. Wigner distribution a nicely fits with the four-particle rapidity gap distribution for the

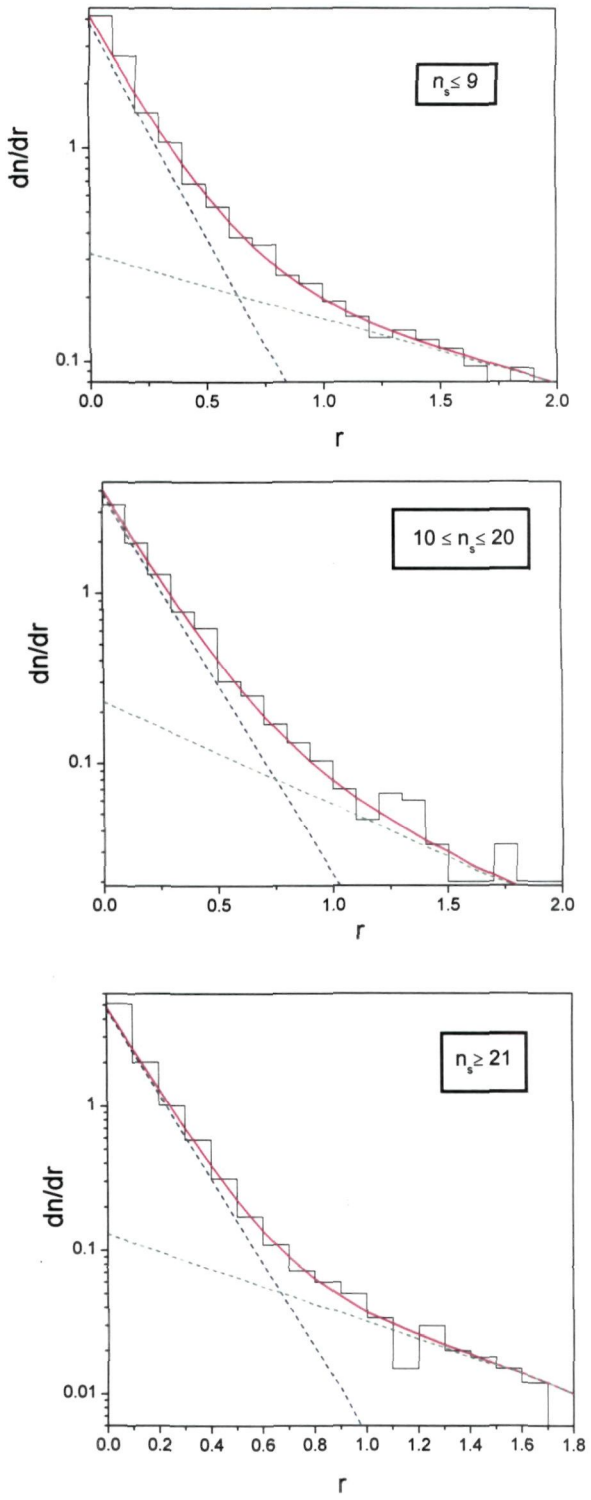

Fig.4.5 Two-particle rapidity gap distributions in 14.5A GeV/c ^{28}Si-nucleus interactions

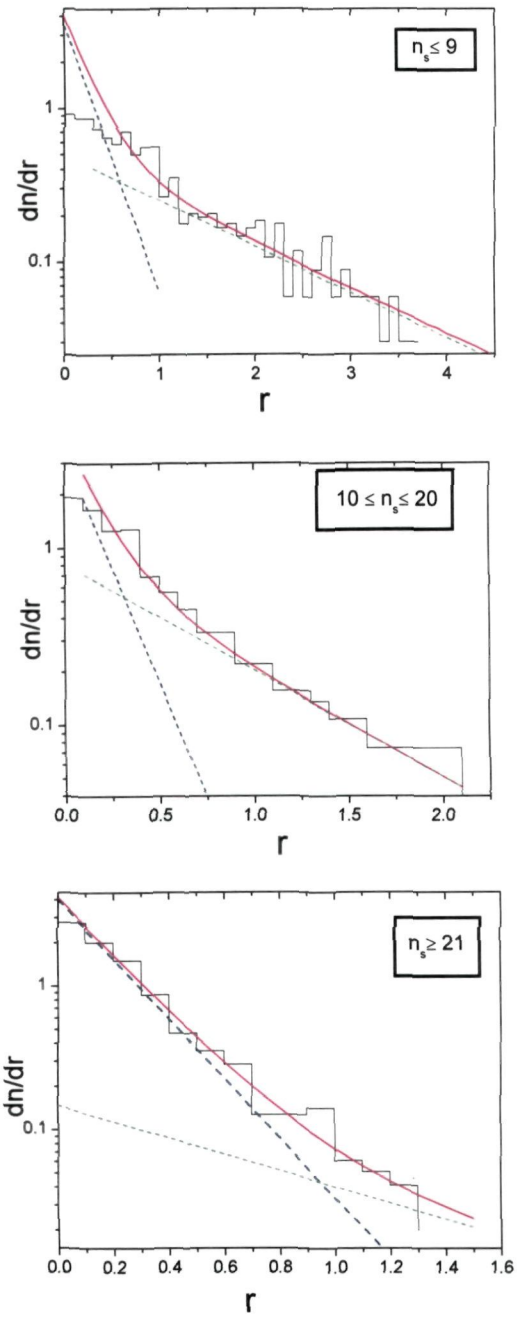

Fig.4.6 Three-particle rapidity gap distributions in 14.5A GeV/c ^{28}Si-nucleus interactions.

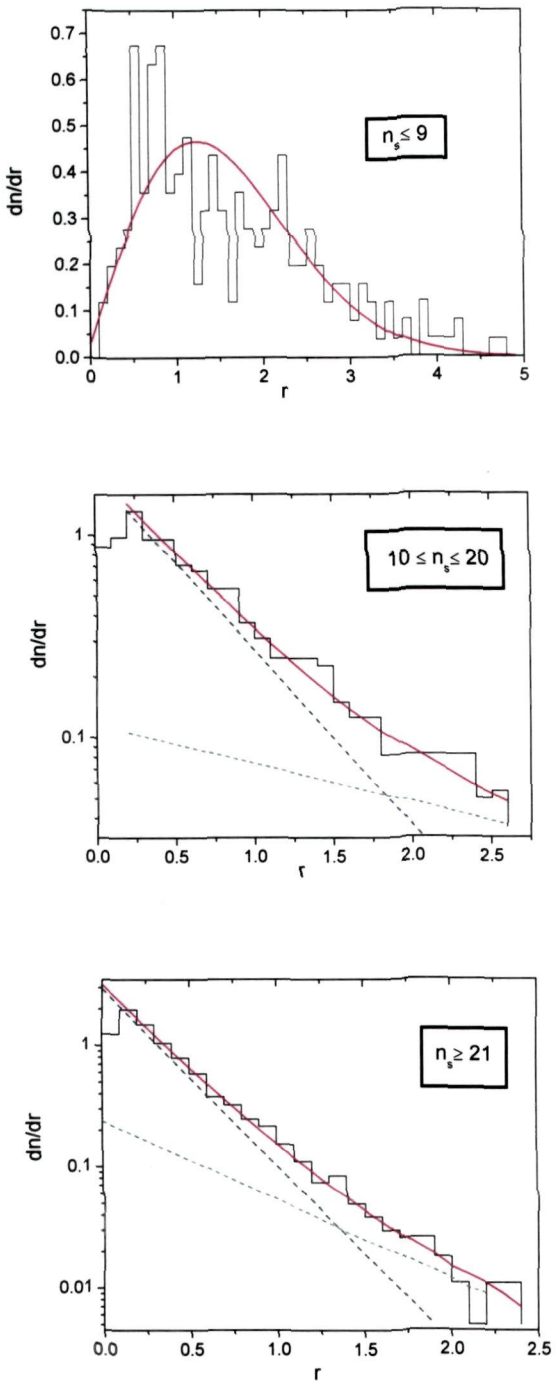

Fig.4.7 Four-particle rapidity gap distributions for 14.5A GeV/c ^{28}Si-nucleus interactions

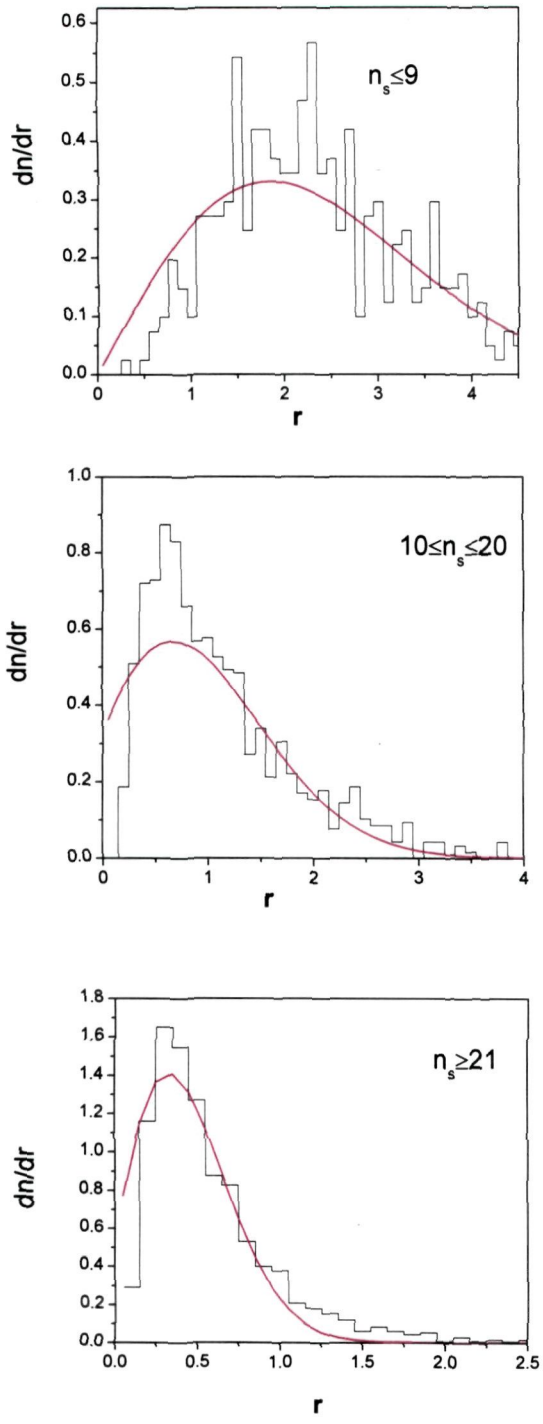

Fig.4.8 Five-particle rapidity gap distributions for 14.5 A GeV/c ^{28}Si-nucleus interactions.

interactions having $n_s \leq 9$ and five-particle rapidity gap distributions,Fig 4.8 for all the three n_s-bins.For each fit the values of χ^2/D.F. are given in Table 4.2.

Table4.2

Values of the parameters occurring in Eq.(4.1) obtained for 14.5A GeV/c ^{28}Si-nucleus interactions in different n_s intervals.

Cluster size	A	B	C	D	χ^2/D.F	χ^2/D.F(Wigner dist.)
$n_s \leq 9$						
Two-particle	4.00±0.44	4.40±0.30	0.35±0.03	0.69±0.02	0.24	-
Three-particle	4.10±0.39	3.90±0.28	0.18±0.01	1.37±0.05	0.15	-
Four-particle	-	-	-	-	-	0.10
Five-particle	-	-	-	-	-	2.15
$10 \leq n_s \leq 20$						
Two-particle	4.20±0.39	4.98±0.40	0.60±0.02	0.70±0.02	0.28	-
Three-particle	3.67±0.22	4.40±0.65	0.23±0.02	1.92±0.31	0.10	-
Four-particle	3.82±0.04	3.93±0.12	0.18±0.01	1.39±0.68	0.13	-
Five-particle	-	-	-	-	-	1.13
$n_s \geq 21$						
Two-particle	3.66±0.42	6.54±0.20	0.42±0.03	0.87±0.03	0.15	-
Three-particle	3.39±0.20	4.72±0.10	0.32±0.02	0.83±0.07	0.13	-
Four-particle	4.09±0.10	2.94±0.32	0.37±0.05	0.93±0.01	0.14	-
Five-particle	-	-	-	-	-	0.82

References:

1. D. R. Snider, Phys. Rev. D11 (1975) 140.

2. G. F. Chew and A. Pignotti, Phys. Rev. 176 (1968) 2112.

3. E. L. Beger, Nucl. Phys. B 85 (1975) 61.

4. N.Ahmad, M.M.Khan, S.Ahmad, M.Zafar and M.Irfan;International J. of Mod. Phys.E,Volume 14,Number4 (2005).

5. A.Shakeel, W.B.Tak, N.Ahmad, A.R.Khan, M.Zafar and M.Irfan;International J. of Mod. Phys.E,Volume 8,No.2 (April 1999)121-129.

6. Tauseef Ahmad, M.Tariq, M.Irfan and H.Khushnood.,Journal of the Physical Soc.of Japan;Vol.56,No.8(1987)2689-2696.

7. M.Irfan, H.Khushnood, A.shakeel, M.Zafar and M.Shafi, Phys. Rev.D30 (1984) 218.

8. A.Shakeel,H.Khushnood, M.Irfan, A.Ahmad, A.H.Naqvi and M.Shafi, Phys.Soc. Japan 55 (1986)3362.

9. H.Khushnood, A.Shakeel, M.Irfan, A.Ahmad and M.Shafi, Phys. Soc. Japan 54 (1985) 2436.

10. Tauseef Ahmad, M.Irfan and M.Shafi, Nuovo Cim. 104A(1991) 1777.

11. Nazeer Ahmad : Ph.D. Thesis submitted to Aligarh Muslim University,Aligarh (2002).

CHAPTER V

Summary and Conclusions

For the last more than 25 years, physicists have been carrying out experiments by colliding heavy ions to understand various interesting features of nucleus-nucleus collisions. These experiments have been performed by gathering evidence from several experiments for studying the behaviour of several observables.

The study of emission characteristics of the produced particles is considered to be of much importance because such studies, if done in a systematic and organized manner, can give deep insight into the underlying mechanism of multiparticle production. The study of mean multiplicities of different types of secondary particles has revealed that the mean multiplicity of relativistic charged particles, $\langle n_s \rangle$, depends strongly on the masses of the projectile as well as target nuclei. Also, $\langle n_s \rangle$ is found to increase rapidly with incident energy, whereas the values of $\langle n_b \rangle$ and $\langle n_g \rangle$, within error limits, are found to be independent of the projectile energy. However, the values of $\langle n_b \rangle$ and $\langle n_g \rangle$ are found to depend on the mass of the target nuclei. The dependence of multiplicity distribution on target mass is found to be, as expected, broader for the heavier targets as compared to the lighter ones. Also, it is found that the Negative Binomial Distribution (NBD) reproduces the multiplicity distribution of relativistic charged particles, n_s and compound multiplicity, n_c , very well.

Study of correlations amongst the produced particles clearly reveal a linear dependence between the mean multiplicity of heavily ionizing particles and n_s.

Also, $\langle n_h \rangle$ and $\langle n_c \rangle$ are found to be strongly correlated with n_s in comparison to $\langle n_b \rangle$ and $\langle n_g \rangle$.

The pseudorapidity distribution of relativistic charged particles was obtained and it was found that the distribution is nicely fitted by Gaussian distribution. To see the dependence of η distribution on the multiplicity of relativistic charged particles, n_s, η spectra of relativistic charged particles was plotted for three different n_s intervals : i) $n_s \leq 9$, ii) $10 \leq n_s \leq 20$ and iii) $n_s \geq 21$. All the three distributions exhibit a sharp peak in the central region of η spectrum, thereby, implying that the central part of η distribution is enriched with particles. A plot of average value of pseudorapidity, $\langle \eta \rangle$, for the three intervals of n_s reveals certain interesting features. For each distribution, the peak shifts towards lower values of $\langle \eta \rangle$ with increasing n_s and height of the peak also increases with increasing n_s.

The clustering of particles can be studied by the dispersion of the rapidity distribution, D(η). Each D(η) distribution for above three n_s intervals exhibits a peak in the central part of the D(η) distribution, indicating thereby the occurrence of clusters. The distribution of shower widths, R(η), has a clear and distinct peak in the mid shower-width region and the peak of R(η) distribution is observed to shift towards higher values of R(η) with increasing multiplicity of relativistic charged particles.

To study correlations amongst the secondary produced particles, the behaviour of the rapidity gap distributions between the n_{th} nearest neighbours are examined and the plots are fitted using Snider's model. From these studies, it can be concluded that in these collisions an intermediate cluster is formed before

finally decaying into real physical particles. The dependence of cluster size on target and multiplicity of the relativistic charged particles has been studied. Two-,three- and four-particle rapidity gap distributions show clear and discernible peaks, whereas no such peak is observed in the case of five-particle rapidity gap distribution, thereby indicating that the maximum number of relativistic charged particles constituting a cluster may be four. Also, this number is found to be essentially independent of the target size. For the events with $n_s \leq 9$, the maximum number of relativistic charged particles constituting a cluster is found to be three, whereas for the interactions with $n_s \geq 10$, this number is turns out to be four. From this result we can conclude that cluster size strongly depends on the multiplicity of relativistic charged particles.